

1  
2  
3  
4  
5  
6  
7  
8  
9  
10  
11  
12  
13  
14  
15  
16  
17  
18  
19  
20  
21  
22  
23  
24

# **The role of melt composition on aqueous fluid vs. silicate melt partitioning of bromine in magmas**

Anita Cadoux<sup>a,b,c,d</sup>, Giada Iacono-Marziano<sup>a,b,c</sup>, Bruno Scaillet<sup>a,b,c</sup>, Alessandro Aiuppa<sup>e,f</sup>,  
Tamsin A. Mather<sup>g</sup>, David M. Pyle<sup>g</sup>, Etienne Deloule<sup>h</sup>, Emanuela Gennaro<sup>a,b,c,f</sup>, Antonio  
Paonita<sup>e</sup>

<sup>a</sup> Université d'Orléans, ISTO, UMR 7327, 45071, Orléans, France

<sup>b</sup> CNRS, ISTO, UMR 7327, 45071 Orléans, France

<sup>c</sup> BRGM, ISTO, UMR 7327, BP 36009, 45060 Orléans, France

<sup>d</sup> GEOPS, Univ. Paris-Sud, CNRS, Université Paris-Saclay, 91405 Orsay, France

<sup>e</sup> Istituto Nazionale di Geofisica e Vulcanologia, Sezione di Palermo, Italy

<sup>f</sup> DiSTeM, Università di Palermo, Italy

<sup>g</sup> Department of Earth Science, University of Oxford, Oxford OX1 3AN, United Kingdom

<sup>h</sup> CNRS, CRPG, Université de Lorraine, UMR 7358, BP 20, 54501 Vandoeuvre-lès-Nancy Cedex, France

Corresponding author: Anita Cadoux

E-mail: [anita.cadoux@u-psud.fr](mailto:anita.cadoux@u-psud.fr)

Revised manuscript for publication in *EPSL*

## 25 **Abstract**

26 Volcanogenic halogens, in particular bromine, potentially play an important role in the ozone  
27 depletion of the atmosphere. Understanding bromine behaviour in magmas is therefore crucial  
28 to properly evaluate the contribution of volcanic eruptions to atmospheric chemistry and their  
29 environmental impact. To date, bromine partitioning between silicate melts and the gas phase  
30 is very poorly constrained, with the only relevant experimental studies limited to investigation  
31 of synthetic melt with silicic compositions. In this study, fluid/melt partitioning experiments  
32 were performed using natural silicate glasses with mafic, intermediate and silicic  
33 compositions. For each composition, experiments were run with various Br contents in the  
34 initial fluid (H<sub>2</sub>O-NaBr), at T - P conditions representative of shallow magmatic reservoirs in  
35 volcanic arc contexts (100-200 MPa, 900-1200°C). The resulting fluid/melt partition  
36 coefficients ( $D_{\text{Br}}^{\text{f/m}}$ ) are:  $5.0 \pm 0.3$  at 1200°C -100 MPa for the basalt,  $9.1 \pm 0.6$  at 1060°C -  
37 200 MPa for the andesite and  $20.2 \pm 1.2$  at 900°C - 200 MPa for the rhyodacite. Our  
38 experiments show that  $D_{\text{Br}}^{\text{f/m}}$  increases with increasing SiO<sub>2</sub> content of the melt (as for  
39 chlorine) and suggest that it is also sensitive to melt temperature (increase of  $D_{\text{Br}}^{\text{f/m}}$  with  
40 decreasing temperature). We develop a simple model to predict the S-Cl-Br degassing  
41 behaviour in mafic systems, which accounts for the variability of S-Cl-Br compositions of  
42 volcanic gases from Etna and other mafic systems, and shows that coexisting magmatic gas  
43 and melt evolve from S-rich to Cl-Br enriched (relative to S) upon increasing degree of  
44 degassing. We also report first Br contents for melt inclusions from Etna, Stromboli, Merapi  
45 and Santorini eruptions and calculate the mass of bromine available in the magma reservoir  
46 prior to the eruptions under consideration. The discrepancy that we highlight between the  
47 mass of Br in the co-existing melt and fluid prior to the Merapi 2010 eruption (433 and 73  
48 tons, respectively) and the lack of observed BrO (from space) hints at the need to investigate  
49 further Br speciation in 'ash-rich' volcanic plumes. Overall, our results suggest that the Br

50 yield into the atmosphere of cold and silicic magmas will be much larger than that from hotter  
51 and more mafic magmas.

52

53 **Keywords:** bromine, fluid/melt partitioning, degassing, arc magmas, atmospheric chemistry

## 54 **1. Introduction**

55 Volcanic degassing is an important process in sustaining the composition of Earth's  
56 atmosphere (e.g., Gaillard and Scaillet, 2014; Mather, 2015). Whilst much progress has been  
57 made constraining global volcanic fluxes, uncertainties remain regarding the emissions of the  
58 key halogen species, especially the trace Br- and I-bearing species (Pyle and Mather, 2009).  
59 However, improvements in remote sensing techniques and analytical techniques, and their  
60 application to an increasing number of active volcanoes, have provided new data on the  
61 concentrations of these minor components in volcanic gases (e.g., Gerlach, 2004; Aiuppa et  
62 al., 2005; Aiuppa, 2009; Bobrowski et al., 2015), which in turn can be used to better constrain  
63 their global fluxes to the atmosphere (Pyle and Mather, 2009). Bromine has received  
64 particular attention over the last decade, owing to its important role in atmospheric chemistry  
65 in general (e.g., Oppenheimer et al., 2006; Roberts et al., 2009; 2014) and ozone depletion in  
66 the troposphere and stratosphere in particular (von Glasow et al., 2009; Kutterolf et al., 2013;  
67 Cadoux et al., 2015). Global compilations show that Br sources (emissions to the atmosphere)  
68 and sinks (removal routes from the atmosphere) are not strictly balanced, hinting at a missing  
69 natural source of Br (Montzka et al., 2011). The direct detection of HBr and BrO in volcanic  
70 plumes (Bobrowski et al., 2003; Aiuppa et al., 2005) suggests that volcanic activity may be  
71 one such a source.

72 The correct evaluation of the contribution of past volcanic eruptions to atmospheric chemistry  
73 depends on our ability to evaluate Br behaviour in magmas, in particular its partitioning  
74 between silicate melt and gas phases. So far, only a few experimental studies have been  
75 performed on this topic, and have investigated Br behaviour in synthetic albite to rhyolite melt  
76 compositions (Bureau et al., 2000; Bureau and Métrich, 2003). However, natural silicate melt  
77 compositions can depart significantly from such model systems, in particular by having  
78 elevated contents of Fe, Mg or Ca, which (as Na) can complex with halogens thereby

79 enhancing their solubility in silicate melts (Cochain et al., 2015). The relationship between  
80 halogen solubility and their complexation with cations has been shown for Cl; chlorine  
81 solubility in most silicate melts is dominantly controlled by the abundances of Mg ~ Ca > Fe  
82 > Na > K > network-forming Al > Li ~ Rb ~ Cs, but Ti, F, and P also have strong influences  
83 (e.g., Webster et al., 1999; Webster and De Vivo, 2002). There is thus a need to evaluate the  
84 role of melt composition on Br behaviour in magmas, which is the main motivation of the  
85 present study. To that end, we have performed fluid/melt partitioning experiments on natural  
86 basalt, andesite and rhyodacite compositions under P-T-H<sub>2</sub>O-redox storage conditions  
87 relevant to shallow arc magmas. Combining our Br partition coefficient for the basaltic  
88 composition, with other experimental data on S and Cl behaviour, and volcanic gas  
89 compositions from the literature, we develop a simple first-order model to predict the S-Cl-Br  
90 degassing behaviour in mafic systems. We also measure Br contents of melt inclusions from  
91 Etna, Stromboli, Merapi and Santorini eruptions and estimate the mass of bromine in the pre-  
92 eruptive magmas, this allows us to address the atmospheric contribution of open-vent mafic  
93 volcanoes versus that of intermediate-silicic volcanoes.

94

## 95 **2. Fluid/melt partitioning experiments**

96

### 97 *2.1 Starting material*

98 The selected starting materials are natural volcanic rocks: a hawaiitic basalt from a 2002 Etna  
99 eruption (Lesne et al., 2011a, b; Iacono-Marziano et al., 2012), a calc-alkaline andesite and a  
100 rhyodacite from the Santorini Upper Scoria-2 (USC-2) and Minoan eruptions, respectively  
101 (Cadoux et. al., 2017). The whole-rocks were crushed and ground in an agate mortar. About  
102 10 g of the powders were melted twice (and ground in between), to ensure homogenization, in  
103 a platinum crucible at 1400 °C - 1 atm for 3-4 hours in a piezoceramic oven, and quenched in

104 cold water. The resulting dry glasses were ground to powder and constituted the starting  
105 material for both (i) bromine standard glasses synthesis (Cadoux et al., 2017) used to calibrate  
106 bromine analyses (section 3) and (ii) partitioning experiments. The compositions of the  
107 starting glasses are given in Table 1.

108

## 109 *2.2 Experimental procedure*

110 Equilibrium partitioning experiments (neglecting kinetic effects) were performed in an  
111 Internally Heated Pressure Vessel equipped with a rapid quench device at the Institut des  
112 Sciences de la Terre d'Orléans (ISTO, Orléans, France). The chosen experimental T-P- $fO_2$   
113 conditions are representative of those in shallow crustal reservoirs in volcanic arc contexts  
114 (Martel et al., 1999; Di Carlo et al., 2006; Cadoux et al., 2014; Kahl et al., 2015) and are  
115 reported in Table 2: T ( $\pm 10^\circ\text{C}$ ) = 900, 1060 and 1200°C, P ( $\pm 2$  MPa) = 100 and 200 MPa,  
116 and  $fO_2$  estimated around the Ni-NiO (NNO) buffer, on the basis of the partial pressure of  $H_2$   
117 imposed in the vessel ( $\sim 2$  bars; Di Carlo et al., 2006; Cadoux et al., 2014).

118 We deliberately used a fluid solely composed of  $H_2O$  and Br. Experiments with simplified  
119 fluids are necessary for comparison with future experiments which will include additional  
120 volatile species (e.g.,  $CO_2$ , S), and will permit us to assess whether or not the presence of  
121 other volatile species can modify Br behaviour.

122 Capsules were always loaded so that the mass ratio between the aqueous fluid and the glass  
123 (silicate) phases was equal to or lower than 0.1 (Table 2), which avoids significant silicate  
124 dissolution into fluid during experiments. About 50 to 100 mg of glass powder was loaded  
125 into Au or Au-Pd capsules (2.5 mm internal diameter, 20-30 mm in length) together with 3-8  
126 mg of a solution composed of distilled water and dissolved NaBr salt. These amounts of  
127 solution (6-10 wt%) ensure the attainment of fluid saturation of the silicate melts at the  
128 investigated T-P conditions. Different solutions with Br contents between 0.1 and 14 wt% Br

129 were employed. The runs lasted between 24 and 92 hours, depending on the temperature  
130 (Table 2). Chlorine partitioning experiments of Alletti et al. (2009) performed at 1200°C with  
131 a basaltic melt showed that 3-4 hours were sufficient to attain equilibrium at 1200°C and  $P >$   
132 1 MPa. Considering that Br diffusion coefficient appears to be 2–5 times lower than the other  
133 halogens in basaltic melts (at 500 MPa to 1.0 GPa, 1250 to 1450 C and at anhydrous  
134 conditions, Alletti et al., 2007), we chose a 24 hour run duration for our experiments at  
135 1200°C-100 MPa including the basaltic composition, to ensure the attainment of equilibrium.  
136 For our experiments at 900°C- 200 MPa including the silicic composition, a run duration of  
137 92 hours was chosen on the basis of previous experiments with chlorine. Kravchuk and  
138 Keppler (1994) performed partitioning experiments with silicic melts at lower T (800°C) and  
139 same P with duration varying between 93h to 1142h, which yielded similar results, thus  
140 demonstrating that 93h was sufficient to attain equilibrium (at 800°C).  
141 The run duration for the experiment at 1060°C (48h) with andesite and rhyodacite  
142 compositions was chosen as intermediate between that at 900°C and that at 1200°C.  
143 Experiments were terminated by drop quench (Di Carlo et al., 2006). Upon opening the  
144 capsules, hissing and fluid escape occurred, indicating the presence of excess fluid, and thus  
145 that fluid saturation was achieved at the target P-T conditions. All runs produced crystal-free  
146 glasses, those of rhyodacitic composition being rich in fluid inclusions (Fig. A.1 in  
147 Supplementary Material).

148

### 149 **3. Analytical techniques**

150

#### 151 *3.1. Major element analysis*

152 Experimental glasses and natural melt inclusions were analysed for their major elements by  
153 electron microprobe (EMP) using the joint ISTO-BRGM SX-Five microbeam facility

154 (Orléans, France). The operating conditions were: 15 kV accelerating voltage, 4-6 nA beam  
155 current, 10 seconds counting time on peaks, 5 seconds on background. The standards used  
156 were: albite for Si and Na,  $\text{TiMnO}_3$  for Ti and Mn,  $\text{Al}_2\text{O}_3$  for Al,  $\text{Fe}_2\text{O}_3$  for Fe, MgO for Mg,  
157 andradite for Ca and orthose for K. Alkalis were analyzed first and a defocused beam was  
158 used to minimize alkali migration: 20  $\mu\text{m}$  diameter for experimental glasses, and 6-10  $\mu\text{m}$  for  
159 melt inclusions. Between 5 and 10 analyses were performed on each charge. The EMP  
160 detection limit for Na (component of the aqueous solution used in the experiments and thus  
161 considered in the calculation of the Br partition coefficients; Supplementary Information) was  
162 generally < 700 ppm.

163

### 164 3.2. *Volatile analysis*

165 Br abundances in the experimental glasses were determined either by Laser Ablation  
166 Inductively Coupled Plasma Mass Spectrometry (LA-ICP-MS) or with a Secondary Ion Mass  
167 Spectrometer (SIMS), using Br glass standards synthesized with the same starting  
168 compositions as those used for the partitioning experiments presented here (Table 1, Cadoux  
169 et al., 2017). LA-ICP-MS has been shown to be a technique suited to analyse Br contents of  
170 hundreds to thousands ppm in experimental glasses, while SIMS and synchrotron X-ray  
171 fluorescence (SR-XRF) are more appropriate techniques for lower Br contents (Cadoux et al.,  
172 2017). Moreover, the spatial resolutions of SIMS and SR-XRF are significantly higher than  
173 that of LA-ICP-MS (Cadoux et al., 2017), we therefore analysed bromine contents in melt  
174 inclusions from Santorini, Merapi and Etna volcanoes by SIMS and SR-XRF.

175 The abundance of water dissolved in most of the experimental glasses was determined by  
176 SIMS.

177

#### 178 3.2.1. *Bromine analysis by LA-ICP-MS*

179 LA-ICP-MS analyses were performed at the Istituto Nazionale di Geofisica e Vulcanologia  
180 (INGV, Palermo, Italy). The laser used is a Compex Pro 102, 193 nm ArF excimer laser  
181 mounted on an ablation system GeoLas Pro, which is connected to an Agilent 7500ce ICP-  
182 MS. Analyses were done on polished glass chips set in epoxy resin.

183 Analyses were performed with a fluence of 15 J/cm<sup>2</sup> and a pulse energy of 100 mJ. The  
184 samples were ablated during ~50 seconds on a 90 µm diameter area, with a pulse repetition  
185 rate of 10 Hz. Three to ten analyses were collected for every sample, to check sample  
186 homogeneity. With this configuration, Br contents of >100 ppm are quantifiable with  
187 accuracy generally within 20% (Cadoux et al., 2017).

188 Data reduction was performed using GLITTER™ software (Griffin et al., 2008), using <sup>24</sup>Mg  
189 as the reference element (Mg contents from EMP analyses), and in-house bromine glass  
190 standards B3000 and B6000 (with 2694 ± 5.1 and 5968 ± 3.5 ppm Br, respectively; Cadoux et  
191 al., 2017), as external standards. The error on the measured <sup>79</sup>Br/<sup>24</sup>Mg ratio was always < 4%.

192

### 193 3.2.2. Bromine analysis by SIMS

194 Polished chips of experimental glasses were set into indium and coated with gold, while  
195 individual crystals from Santorini Minoan eruption, Merapi 2010 eruption and Etna 2006  
196 eruption were mounted in epoxy resin, polished and coated with gold for melt inclusion  
197 analysis.

198 Analyses were conducted at the Centre de Recherches Pétrographiques et Géochimiques  
199 (CRPG, Nancy, France) with a Cameca IMS 1280 HR2. The Cs<sup>+</sup> primary ion beam was  
200 accelerated at 10 kV with an intensity of 5 nA, and focused on a 15 µm diameter area. The  
201 electron gun was simultaneously used for charge compensation. Negative secondary ions  
202 were extracted with a 10 kV potential, and the spectrometer slits set for a mass resolving  
203 power (MRP = M/ΔM) of ~20,000. A single collector (EM) was used in ion-counting mode,

204 and the spectrum scanned by peak jumping. Each analysis consisted of 8 or 6 successive  
205 cycles. Each cycle began with background measurement at the mass 75.8, followed by  
206  $^{28}\text{Si}^{16}\text{O}_3^-$  (75.963 amu),  $^{30}\text{Si}^{16}\text{O}_3^-$  (77.959 amu),  $^{79}\text{Br}^-$  and  $^{81}\text{Br}^-$ , with measurement times of 4,  
207 4, 4, 10 and 30 s, respectively (waiting time of 2 s). More details about the analytical  
208 configuration can be found in Cadoux et al. (2017).

209 We used three different sets of in-house bromine glass standards (Cadoux et al., 2017): a  
210 basaltic set containing 1 to 6,000 ppm Br (B1 to B6000), an andesitic set containing 10 to  
211 1,000 ppm Br (A10 to A1000), and a rhyodacitic set containing 10 to 5,000 ppm Br (RD10 to  
212 RD5000).

213 The bromine content of the samples was calculated using the measured  $^{81}\text{Br}/^{28}\text{SiO}_3$  and  
214 known Br (ppm)/ $\text{SiO}_2$  (wt%) ratios of the standards (Cadoux et al., 2017).

215 The three glass sets define distinct linear calibration curves with slopes decreasing with  
216 increasing degree of melt polymerization (Cadoux et al., 2017). The equation of the  
217 calibration lines passing through zero is:

$$\left(\frac{^{81}\text{Br}}{^{28}\text{SiO}_3}\right) = a \left(\frac{\text{Br}}{\text{SiO}_2}\right)$$

218 where the slope  $a$  is a function of  $\text{SiO}_2$  content.

219 The error on the measured  $^{81}\text{Br}/^{28}\text{SiO}_3$  ratio was generally  $< 3\%$  (most often  $< 2\%$ ).

220

### 221 3.2.3. *Br analysis by SR-XRF*

222 Bromine in Etna and Stromboli melt inclusions was analysed via SR-XRF at the UK  
223 national synchrotron facility, Diamond Light Source (Didcot, Oxfordshire), on I18, the  
224 Microfocus Spectroscopy beamline. Analyses were performed on polished olivine-hosted  
225 melt inclusions set in epoxy resin, using a beam of  $\sim 5 \times 5 \mu\text{m}^2$  and an analysis time of 120 s  
226 (details in Cadoux et al., 2017). Fluorescence spectra were processed by PyMca (Solé et al.,

227 2007), by identifying the K-lines of Br and applying an iterative Gaussian peak fitting  
228 procedure to quantify the net peak areas free of background and interference from other  
229 elements.

230 Background- and baseline-subtracted net peak areas for the MI samples were converted into  
231 Br concentrations from comparison with peak areas measured for the basaltic standards of  
232 known Br composition (Cadoux et al., 2017). Based on tests made on the standards (Cadoux  
233 et al., 2017), the Br detection limit is inferred to be  $< 1$  ppm, Br contents  $\leq 5$  ppm  
234 (representative of Br contents in most natural volcanic glasses) are measured with an accuracy  
235  $< 26\%$  and with a precision of  $30\%$ .

236

#### 237 3.2.4. *Water analysis by SIMS*

238 The analysis of water dissolved in the experimental glasses was performed on the CRPG  
239 Cameca 1280 HR2. Spot analyses of secondary ions  $^{17}\text{O}$ ,  $^{16}\text{O}^1\text{H}$ ,  $^{18}\text{O}$ ,  $^{29}\text{Si}$ ,  $^{30}\text{Si}$  were obtained  
240 using a 3 nA, 20  $\mu\text{m}$  diameter primary beam of  $\text{Cs}^+$  ions. The electron gun was  
241 simultaneously used for charge compensation. The measurements were made at a mass  
242 resolution of  $\sim 7,700$  to separate  $^{17}\text{O}^-$  and  $^{16}\text{O}^1\text{H}^-$ . An energy filtering was set at  $+30 \pm 10$  eV in  
243 moving the energy slit off axis, to minimize both matrix effect and instrumental background.  
244 A  $10 \times 10$   $\mu\text{m}$  raster was used for 1 minute prior to analysis at each spot in order to pre-  
245 sputter through the gold coat and remove surface contamination. The beam position in the  
246 field aperture and the magnetic field centering was checked before each measurement. Each  
247 analysis on one spot consisted of 18 cycles of measurements, with counting times and  
248 switching times of 3 and 1 s respectively at each peak. The errors on the measured  $^{16}\text{O}^1\text{H}/^{30}\text{Si}$   
249 ratios were  $< 1\%$ .

250 Concentrations of  $\text{H}_2\text{O}$  were calculated using a best-fit quadratic polynomial regression to  
251 count-rate ratios (normalized to  $^{30}\text{Si}$ ) versus variable known concentration ratios (referenced

252 to wt% SiO<sub>2</sub>) of experimental glass standards of basaltic (sample N72, Kamtchatka; Shishkina  
253 et al., 2010), trachy-andesitic (sample TAN25, Tanna Island, Vanuatu; Metrich & Deloué,  
254 2014), dacitic and rhyolitic (Pinatubo, Philippines; Scaillet & Evans, 1999) compositions,  
255 with H<sub>2</sub>O contents ranging from 0 to ~6 wt%.

256

## 257 **4. Results**

### 258 *4.1. Major element compositions*

259 Average major element compositions of experimental glasses and melt inclusions are  
260 presented in Tables 3 and A2, respectively. Comparison of the experimental products (Table  
261 3) with the corresponding starting dry glasses (Table 1) shows a systematic gain in Na<sub>2</sub>O due  
262 to the addition of sodium through the H<sub>2</sub>O-NaBr solution in the experimental charges (10 to  
263 153 µg of Na were incorporated into the final glass, Table A.1), and a loss in FeO (up to 14%  
264 taking into account standard deviations) in experiments  $\geq 1060$  °C, most likely due to Fe  
265 alloying with the AuPd capsule. Other elements were generally comparable with the starting  
266 glasses within standard deviations.

267

### 268 *4.2. H<sub>2</sub>O and Br dissolved in experimental glasses*

269 The concentrations of both H<sub>2</sub>O and Br dissolved in quenched glasses are reported in Table  
270 2. Melt water contents (H<sub>2</sub>O<sub>melt</sub>) vary between 2.9 up to 7.3 wt%, encompassing the range of  
271 pre-eruptive H<sub>2</sub>O<sub>melt</sub> of arc magmas (e.g., Scaillet et al., 1998; Di Carlo et al., 2006; Cadoux et  
272 al., 2014). Bromine concentrations range from 69 (M4-RD1; Table 2) to 9112 ppm (M2-B),  
273 comparable to the range explored in previous experimental studies (Bureau et al., 2000;  
274 Bureau and Métrich, 2003). Repeat analyses of either H<sub>2</sub>O (n = 5-7) or Br (n = 3-10) in  
275 quenched glasses show them to be homogeneous within analytical uncertainty (including error  
276 on calibration and error on sample measurements), indicating that the run durations (1 to 4

277 days according to T-P conditions; Table 2) were sufficient to attain chemical equilibrium  
278 between the co-existing melt and fluid phases.

279

#### 280 4.3. *Fluid/melt bromine partitioning*

281 Assessment of the partition coefficients requires the calculation of the ratio between Br  
282 concentration (in ppm) in coexisting aqueous fluid and silicate melt at the experimental  
283 conditions. In natural magmatic systems, besides from being dissolved in the silicate melt, Br  
284 can exist as a gas species in the vapour phase and/or be dissolved in hydrosaline liquid phase  
285 (brine), as has been shown for Cl. This raises the question as to whether a brine rich in Br  
286 could have been present in our capsules at run conditions. Solubility experiments of Bureau et  
287 al. (2003) have shown that silicic melts can contain up to 7850 ppm Br at P-T conditions of  
288 100-200 MPa and 900-1080°C without brine occurrence. Our experiments were run at similar  
289 conditions, with Br contents lower than 2000 ppm (Table 2). We thus conclude that our silicic  
290 melts did not co-exist with a brine, and that only a gas phase was present. There is no data  
291 about Br solubility in mafic melts but the results of our experiment #3 (basalt, andesite,  
292 rhyodacite in the same experimental P-T-H<sub>2</sub>O-[Br<sup>o</sup>] conditions; Table 2) suggest a higher  
293 ability for Br to enter in mafic melts, so that, by comparison with the values for silicic melts  
294 given above, we might expect that brine saturation in andesitic and basaltic melts occurs for  
295 Br contents higher than 8000 ppm. Hence, as for the silicic melts, we conclude that basaltic-  
296 andesitic charges were co-existing solely with a gas phase during the experiments.

297 Whereas the amount of Br dissolved in the melt ([Br]<sub>melt</sub>) was directly analysed (by SIMS or  
298 LA-ICP-MS in run product glasses, section 3; referred to as '[Br] measured in final glass' in  
299 Table 2), the Br amount of the coexisting aqueous fluid phase ([Br]<sub>fluid</sub>) was determined by  
300 mass balance, knowing the original bulk Br content (the amount of Br loaded in the capsule as  
301 H<sub>2</sub>O+NaBr solution; hereafter [Br<sup>o</sup>]), the measured amount of Br dissolved in the final glass

302 ([Br]<sub>melt</sub>), and assuming that the difference between these two figures represents the amount of  
303 Br left over for the fluid phase.(details of the calculation are given in Supplementary  
304 Information and in Table A.1). For each run product, we estimated the errors on the calculated  
305 [Br]<sub>fluid</sub> and  $D_{\text{Br}}^{\text{f/m}}$  by propagating the errors coming from the preparation of the experimental  
306 charges to the analysis of Br, Na and H<sub>2</sub>O contents of the glasses (Supplementary Information  
307 and Table A.1). The resulting errors on [Br]<sub>fluid</sub> are < 51% (and mostly < 34%), except for one  
308 run-product (M1-B). As the main source of error for  $D_{\text{Br}}^{\text{f/m}}$  is [Br]<sub>fluid</sub>, the resulting errors on  
309  $D_{\text{Br}}^{\text{f/m}}$  are close to those for [Br]<sub>fluid</sub>: they do not exceed 54% and are mostly <45%, except for  
310 M1-B (112%; Table A.1). Note that, as underlined in previous studies (e.g., Alletti et al.,  
311 2014), such rigorous error propagation overestimates the real errors, due to the complex  
312 covariation of individual errors. The large error associated with the  $D_{\text{Br}}^{\text{f/m}}$  estimated for M1-B  
313 is due to the low fluid/melt mass ratio of the experimental charge (0.06 compared to 0.08-0.11  
314 for the others): the mass of initial fluid is small relative to the weighing error (Table A1).  
315 Therefore, the calculated mass of fluid has a larger associated relative error of 19% (<15% for  
316 the other run products), which increases the error on the calculated value for [Br]<sub>fluid</sub> and  
317  $D_{\text{Br}}^{\text{f/m}}$ . This observation is consistent with the uncertainty analysis for the mass balance  
318 calculations of Zajacz et al. (2012), which shows that the determination of D for elements  
319 with low D values in experiments with low volatile/mass ratio may bear large uncertainties  
320 due to error propagation. Their modeling (Fig. 1 in Zajacz et al., 2012) predicts relative error  
321 of 10 up to 100% for volatile/mass ratios lower than 0.1. The error on the  $D_{\text{Br}}^{\text{f/m}}$  estimated for  
322 M1-B being > 100% ( $D_{\text{Br}}^{\text{f/m}} = 3.8 \pm 4.5$ ), we conclude that this value, taken alone, is  
323 meaningless. Overall, the error on  $D_{\text{Br}}^{\text{f/m}}$  is particularly sensitive to the error on the measured  
324 [Br]<sub>melt</sub> (i.e., Br content of the run product glasses). The precision of the Br measurements is  
325 crucial for the accuracy of  $D_{\text{Br}}^{\text{f/m}}$ .

326 The main data of the partitioning experiments are listed in Table 2 (details in Table A1) and  
327 displayed on Figures 1 to 5.

328 The basaltic products of runs #1 to 3 performed at 1200°C, 100 MPa, with various [Br<sup>o</sup>]  
329 contents apparently show a linear relationship between the measured [Br]<sub>melt</sub> and the  
330 calculated [Br]<sub>fluid</sub> (Fig. 1). Linear regression forced through zero yields a  $D_{Br}^{f/m} = 5.0 \pm 0.3$   
331 for the basaltic composition. At the same T-P-[Br<sup>o</sup>] conditions (experiment #3; Table 2),  
332  $D_{Br}^{f/m}$  increases steadily from basalt ( $D_{Br}^{f/m} = 4.6 \pm 2.0$ ), to andesite ( $D_{Br}^{f/m} = 6.4 \pm 3.5$ ), to  
333 rhyodacite ( $D_{Br}^{f/m} = 11.3 \pm 0.9$ ). At 1060°C, 200 MPa, ~NNO (Fig. 2), experiments on  
334 andesite and rhyodacite melts yields linear trends between [Br]<sub>melt</sub> and [Br<sup>o</sup>] (Fig. 2a) or  
335 [Br]<sub>fluid</sub> (Figs. 2b and 2c). Linear regression of the latter data forced through zero yields  $D_{Br}^{f/m}$   
336  $= 9.1 \pm 0.6$  for andesite, and  $D_{Br}^{f/m} = 14.0 \pm 0.6$  for rhyodacite. At 900°C - 200 MPa, (Fig. 3),  
337 the same pattern is again observed resulting in  $D_{Br}^{f/m} = 20.2 \pm 1.2$  for rhyodacite, slightly  
338 higher than that of Bureau et al. (2000) for albitic melts ( $17.5 \pm 0.6$ ).

339 The experiments show a two-fold increase of  $D_{Br}^{f/m}$  from basalt ( $5.0 \pm 0.3$ ) to rhyolite melts  
340 ( $11.3 \pm 0.9$ ) at 1200°C - 100 MPa (Fig. 4). The same trend of an increase of  $D_{Br}^{f/m}$  with SiO<sub>2</sub>  
341 is noted at 1060°C - 200 MPa, with a slightly higher slope. At 900°C, we did not work on  
342 basaltic/andesitic compositions because of their extensive crystallization (which would have  
343 driven the residual liquids toward higher SiO<sub>2</sub> content). Our data on silicic compositions,  
344 along with those of Bureau et al. (2000) (Fig. 4), suggest a similar trend of increasing  $D_{Br}^{f/m}$   
345 with increasing SiO<sub>2</sub> at 900°C. Figure 4 also suggests a general trend of an increase in  $D_{Br}^{f/m}$   
346 as temperature decreases, at least for more silicic compositions. For instance, for rhyolitic  
347 melts (71 wt% SiO<sub>2</sub>), a linear extrapolation of our data set ( $D_{Br}^{f/m} = -0.0299 \times T(^{\circ}C) + 46.673$ ,  
348  $r^2 = 0.97$ ) yields  $D_{Br}^{f/m} = 26$  at 700°C (Fig. 5).

349 We did not attempt to explore the effect of pressure in a systematic way. Previous work has  
350 shown that  $D_{Br}^{f/m}$  strongly increases as pressure decreases, from about 20 at 200 MPa up to

351 over 300 at near atmospheric pressure in silicic melts (synthetic haplogranitic composition;  
352 Bureau et al., 2010). In contrast, our experiment at 100 MPa (experiment #3) does not show  
353 any significant increase in  $D_{\text{Br}}^{f/m}$ , with  $D_{\text{Br}}^{f/m}$  being instead generally lower than those at 200  
354 MPa (experiments #4 and #5; Table 2). However, the fact that temperatures between our 100  
355 and 200 MPa runs are different, does not allow us to make definitive conclusions on this  
356 aspect. We suggest that our results should be used to model degassing processes in the crustal  
357 reservoir and not for simulating decompression processes between the reservoir and surface.

358

#### 359 *4.4. Br contents in melt inclusions*

360 Table A.2 reports the Br contents of melt inclusions from (i) basaltic magmas erupted at  
361 Mount Etna and Stromboli, (ii) the andesitic magma erupted in 2010 at Mount Merapi, and  
362 (iii) the rhyodacitic magma of the 1613 BC Minoan eruption of Santorini volcano. Melt  
363 inclusions from Mt. Etna and Stromboli are hosted by olivine crystals, while those from Mt.  
364 Merapi and Santorini volcano are in pyroxenes and plagioclase crystals, respectively.

365 Br abundance ranges from 2.5 to 10 ppm, without any clear correlation with melt inclusion  
366 major element composition; there is no notable difference between basaltic, andesitic and  
367 rhyodacitic melt inclusions. The Br contents of these melt inclusions are comparable to those  
368 of submarine back-arc and arc glasses (Kendrick et al., 2014).

369

## 370 **5. Discussion and applications**

371

### 372 *5.1. Halogen behaviour*

373 This section aims to place our novel Br partitioning data in the wider framework of  
374 halogen behaviour. Hereafter, we provide a brief, non-exhaustive review of chlorine, fluorine  
375 and iodine partitioning and make comparisons with bromine.

376 Many studies have been dedicated to understanding the partitioning behaviour of halogens  
377 between fluids and silicate melts (e.g., Webster, 1990; Webster and Holloway 1990; Webster  
378 1992a,b; Webster et al. 1999; Signorelli and Carroll, 2000; Bureau et al., 2000; Botcharnikov  
379 et al., 2004, 2007, 2015; Dolejs and Baker 2007a,b; Alletti, 2008; Stelling et al. 2008;  
380 Chevychelov et al., 2008b; Webster et al., 2009; Borodulin et al., 2009; Alletti et al. 2009,  
381 2014; Beermann 2010; Zajacz et al. 2012; Webster et al., 2014; Beermann et al., 2015).  
382 Nevertheless, most of these studies have focused on chlorine, mainly because of its  
383 importance as a ligand for ore metals (e.g., Carroll and Webster, 1994; Aiuppa et al., 2009).

384

#### 385 *5.1.1 General behaviour*

386 Chlorine partitions preferentially into fluids relative to melts for the vast majority of terrestrial  
387 magmas at shallow-crustal pressure and temperature conditions, due to its highly solubility in  
388 aqueous and aqueous-carbonic fluids (e.g., Webster et al., 2018 and references therein). The  
389 few partitioning experiments performed with bromine and iodine show a similar behaviour  
390 (Bureau et al., 2000; Bureau et al., 2016; this study). In contrast, fluorine concentrations in  
391 aqueous and aqueous-carbonic fluids at magmatic conditions are much lower than those of the  
392 other halogens (e.g., Carroll and Webster, 1994), and can be therefore enriched in the silicate  
393 melt with respect to the fluid phase (e.g., Webster, 1990; Webster and Holloway 1990).

394

#### 395 *5.1.2 The effect of melt composition*

396 In this study, we show that the partitioning of bromine between aqueous fluid and melt  
397 appears to be influenced by the melt composition (Figs. 1, 2, 4). We estimate  $D_{\text{Br}}^{f/m}$  of  $4.6 \pm$   
398  $2.0$ ,  $6.4 \pm 3.5$  and  $11.3 \pm 0.9$  for basaltic, andesitic and rhyodacitic compositions respectively,  
399 with  $[\text{Br}^\circ] = 2.4$  wt.%, at 1200°C, 100 MPa and  $f\text{O}_2$  close to NNO (exp. #3, Table 2). If  $D_{\text{Br}}^{f/m}$   
400 of the basalt and andesite are comparable taking into account the error bars, the difference

401 between the mafic-intermediate compositions on one hand, and the silicic composition on the  
402 other hand, is significant. In addition, we observe the same trend at 1060°C, 200 MPa where  
403  $D_{\text{Br}}^{f/m}$  of the silicic composition ( $14.0 \pm 0.6$ ) is significantly higher than that of the  
404 intermediate composition ( $9.1 \pm 0.6$ ). This relationship between melt composition and Br  
405 partitioning is consistent with the higher Br solubility in melts with lower SiO<sub>2</sub> observed by  
406 Bureau and Métrich (2003). The recent study of Cochain et al. (2015) on Br speciation in  
407 hydrous alkali silicic melts at high pressure (up to 7.6 GPa) confirms this trend. Similarly,  
408 several studies have demonstrated the strong effect of melt composition on fluid/melt  
409 partitioning of chlorine (Webster 1992a,b; Webster et al. 1999). Like  $D_{\text{Br}}^{f/m}$ ,  $D_{\text{Cl}}^{f/m}$  also  
410 increases with increasing SiO<sub>2</sub> contents of the melts (i.e., with increasing melt polymerization  
411 and thus decreasing Br and Cl solubility in melt; e.g., Webster, 1992a,b; Signorelli and  
412 Carroll, 2000; Botcharnikov et al., 2004; Webster, 2004; Webster et al., 2006; Webster et al.,  
413 2009). Most experimental values of  $D_{\text{Cl}}^{f/m}$  for basaltic systems are <10 (Stelling et al 2008;  
414 Beermann 2010; Baker and Alletti 2012), but Alletti et al. (2009) observed  $D_{\text{Cl}}^{f/m}$  of 8-34 in  
415 trachybasaltic melt in equilibrium with aqueous fluids at  $f\text{O}_2$  near NNO. Values of  $D_{\text{Cl}}^{f/m}$  for  
416 intermediate (andesitic and phonolitic) and silicic melts exceed those for mafic melts (e.g.,  
417 Webster et al. 1999; Stelling et al., 2008; Chevychelov et al., 2008b; Alletti et al., 2009;  
418 Beermann, 2010; Beermann et al., 2015); with values >160 determined for silicic melts at 200  
419 MPa (Webster, 1992a). Note that  $D_{\text{Cl}}^{f/m}$  also varies strongly with Cl concentration (Webster  
420 1992a,b; Webster et al. 1999; Stelling et al. 2008) and a decrease of  $D_{\text{Cl}}^{f/m}$  by up to the order  
421 of one magnitude can be observed when the Cl concentration in the system decreases (from  
422 several wt.% to <1 wt.% Cl). At low Cl system concentrations (<1 wt% Cl in andesite, Zajacz  
423 et al., 2012; or in basalt, Beermann et al., 2015; Stelling et al., 2008),  $D_{\text{Cl}}^{f/m}$  seems to achieve  
424 values close to or even below unity. From our data, we do not observe any systematic  
425 relationship between Br concentration in the system ( $[\text{Br}^\circ]$ ) and  $D_{\text{Br}}^{f/m}$ : the apparent decrease

426 of D-values for andesite (M4-A) relative to  $[\text{Br}^\circ]$  at 1060°C and 200 MPa (Table 2) is actually  
427 not significant taking into account the errors on D. More experiments are necessary to  
428 investigate the potential relationship between  $D_{\text{Br}}^{f/m}$  and the Br concentration in the system.  
429 Unlike bromine and chlorine, values of  $D^{f/m}$  for fluorine are lower in silicic melts (typically  
430 well below unity; Webster, 1990; Webster and Holloway 1990; Dolejs and Baker 2007a,b;  
431 Borodulin et al., 2009) than in mafic melts coexisting with aqueous fluids (ca. 3 to 38; Alletti,  
432 2008; Chevychelov et al., 2008b).

433

### 434 *5.1.3 Temperature and pressure effects*

435 Our data suggest that  $D_{\text{Br}}^{f/m}$  is sensitive to melt temperature (increase of  $D_{\text{Br}}^{f/m}$  with decreasing  
436 temperature; Figs. 4 and 5), though more experiments are required to confirm this trend.  
437 Currently there are insufficient data available to constrain the temperature effect for the other  
438 halogens. The few existing data concern Cl in phonolitic and trachybasaltic melts and suggest  
439 that there is no strong influence of temperature (Chevychelov et al., 2008a; Stelling et al.,  
440 2008).

441 We do not systematically investigate the effect of pressure on  $D_{\text{Br}}^{f/m}$ . Experiments conducted  
442 on haplogranite melts coexisting with iodine-bearing aqueous fluids indicate an increase of  
443  $D^{f/m}$  of iodine with pressure decrease (from ~2 at 1.5 GPa to 41 at 0.1 GPa; Bureau et al.,  
444 2016). Contrastingly,  $D^{f/m}$  of fluorine decreases with decreasing pressure as suggested by  
445 experiments on trachybasaltic melts (Alletti, 2008; Chevychelov et al., 2008b). Available data  
446 for chlorine show no clear pressure effect on  $D_{\text{Cl}}^{f/m}$  for most compositions and contrasting  
447 effects for phonolitic ones (Signorelli and Carroll, 2000; Baker and Alletti, 2012; Alletti et al.  
448 2014).

449 We conclude that more systematic experiments are necessary for all halogens to assess the  
450 effect of pressure and temperature on their fluid/melt partitioning, in order to interpret  
451 degassing processes of ascending and cooling magmas comprehensively.

452

#### 453 *5.1.4 Effect of fluid composition*

454 Experiments with trachybasaltic melts coexisting with aqueous fluids have shown that the  
455 addition of CO<sub>2</sub> to the system leads significant reductions of  $D^{f/m}$  of fluorine.

456 Several studies have investigated the effect of fluid composition on Cl partitioning in  
457 chemically complex O-H ± C ± S ± Cl fluids and show variable influence of CO<sub>2</sub> or S on  
458  $D_{Cl}^{f/m}$ , no systematic trend appears (e.g., Botcharnikov et al. 2004; Webster et al. 2003;  
459 Botcharnikov et al., 2007; Alletti et al., 2009; Beermann 2010, Zajacz et al. 2012; Webster et  
460 al., 2014). As we do not explore the effect of other volatile species on Br partitioning in this  
461 study, we will not enter into the details of those studies (for a review on this topic, see  
462 Webster et al., 2018). Clearly, further investigations are needed to better understand the  
463 effects of other volatile species on halogens partitioning.

464

#### 465 *5.1.5 Role of ionic radius?*

466 On the basis of their results ( $D_{Cl}^{f/m} = 8.1$ ,  $D_{Br}^{f/m} = 17.5$ ,  $D_I^{f/m} = 104$  with an albitic melt),  
467 Bureau et al. (2000) suggested that bromine and iodine partitioned even more strongly into the  
468 fluid phase than chlorine and that it could be correlated to the increasing ionic radius of the  
469 halide ions ( $Cl^- = 1.81 \text{ \AA}$ ,  $Br^- = 1.96 \text{ \AA}$ ,  $I^- = 2.20 \text{ \AA}$ ; Shannon, 1976). Nevertheless, our brief  
470 review above shows that chlorine fluid/melt partition coefficients as high as that of iodine  
471 may be reached with a rhyodacitic melt ( $D_{Cl}^{f/m} = 115$ , Table 2 in Webster et al., 2009)  
472 depending on the initial Cl content in the bulk system. In addition, we show in section 5.2.  
473 below that the range of Br and Cl composition of volcanic gases and melts from mafic

474 systems requires a lower  $D_{\text{Br}}^{f/m}$  (= 5) than the  $D_{\text{Cl}}^{f/m}$  value (8.6); this questions the general  
475 applicability of the higher volatility of Br as shown by the experimental results of Bureau et  
476 al. (2000) and Mungall and Brenan (2003) and attributed to the larger ionic radius of Br vs.  
477 Cl.

478

## 479 5.2. *S-Cl-Br degassing behaviour in mafic magma systems*

480 Our partition coefficients for Etnean melts set the basis for initializing the first basic  
481 models to evaluate Br degassing behaviour in mafic systems. Our aim is to derive model-  
482 based evidence for Br abundance in magmatic gases coexisting with mafic melts at shallow  
483 crustal conditions, and to compare this with available information on the measured  
484 compositions of volcanic gases, the ultimate product of magmatic degassing. Figure 6a shows  
485 a selection of volcanic gas plume compositions (in the S-Cl-Br system) from some open-vent  
486 mafic volcanoes (for data provenance, see caption of Figure 6). The wide range of volcanic  
487 gas S/Br compositions observed points to a mechanism fractionating Br, relative to sulfur,  
488 during magmatic degassing or systematic variations in melt compositions, e.g., between  
489 different tectonic settings. In comparison, volcanic gases exhibit a far more restricted range of  
490 Cl/Br ratios (see Fig. 6a and Gerlach, 2004; Aiuppa et al, 2005, 2009; Webster et al., 2018),  
491 which suggests that less Cl/Br fractionation takes place during degassing and/or less  
492 comparative variation in melt compositions. The relatively constant Cl/Br ratios in our gas  
493 dataset also indicate that Cl vs. Br decoupling due to fractionations among coexisting brine  
494 and vapour (Foustoukos and Seyfried, 2007; Seo and Zajacz, 2016), or by halite precipitation  
495 (Foustoukos and Seyfried, 2007), are unlikely to occur at the mafic, halogen-poor melt  
496 conditions explored here (Webster et al., 2009, 2018). We consider below our new Br  
497 partitioning data, in tandem with previous information on S and Cl from the literature, to  
498 provide a simple model verification for these volcanic gas-based inferences.

499 Rigorous quantitative calculation of magmatic gas compositions would require a theoretical  
 500 and/or empirical model that describes solubilities, fluid/melt partition coefficient, and  
 501 diffusivities of all involved volatiles over the range of P-T-X conditions experienced by  
 502 magmas upon ascent, storage, and eruption. Such quantitative information is increasingly  
 503 available for S (see review of Baker and Moretti, 2011), still limited for Cl (Webster et al.,  
 504 1999, 2015, 2018), but virtually absent for Br. Given this limitation, we base our model  
 505 calculations on a modified version of the empirical degassing model of Aiuppa et al. (2002)  
 506 and Aiuppa (2009). The original model described the evolution of the SO<sub>2</sub>-HCl-HF magmatic  
 507 gas phase exsolved during progressive degassing of a basaltic magma, using a Rayleigh-type  
 508 open-system degassing model assumption, and with constant S, Cl and F fluid/melt partition  
 509 coefficients. Based on fair agreement between model results and volcanic gas compositions, it  
 510 was concluded that a Rayleigh-type open-system process could suitably reproduce the  
 511 relatively shallow exsolution of halogens from basaltic magmas that often dominates the gas  
 512 signature (Métrich and Wallace, 2008; Métrich et al., 2001, 2004, 2010; Spilliaert et al., 2006;  
 513 Edmonds et al., 2009; Webster et al., 1999, 2015; Mather et al., 2012).  
 514 Here we adapt and extend the methodology of Aiuppa (2009) to bromine, and develop a  
 515 simple model to account for the variability of S-Cl-Br compositions of volcanic gases (Fig.  
 516 6a). We use similar sets of Rayleigh-type open-system equations as in Aiuppa (2009) but,  
 517 contrarily to previous work, we do not derive fluid/melt partition coefficients using an  
 518 empirical best-fit procedure to volcanic gas data, but rather use independent information  
 519 (from Alletti et al., 2009; Aiuppa, 2009; and this work) (see below).  
 520 We use equations (1) and (2) to calculate the evolving S/Cl and S/Br (molar) ratios in the  
 521 magmatic gas phase produced upon increasing extents of degassing of a mafic silicate melt:

$$\left(\frac{S}{Cl}\right)_{\text{gas}} = \left(\frac{S}{Cl}\right)_{\text{melt}_0} \cdot \frac{D_S}{D_{Cl}} \cdot R^{\left(1 - \frac{D_{Cl}}{D_S}\right)} \quad (1)$$

523 
$$\left(\frac{S}{Br}\right)_{\text{gas}} = \left(\frac{S}{Br}\right)_{\text{melt}_0} \cdot \frac{D_S}{D_{Br}} \cdot R^{\left(1 - \frac{D_{Br}}{D_S}\right)} \quad (2)$$

524 where  $\left(\frac{S}{Cl}\right)_{\text{gas}}$  and  $\left(\frac{S}{Br}\right)_{\text{gas}}$  are the molar volatile ratios in the gas phase;  $\left(\frac{S}{Cl}\right)_{\text{melt}_0}$  and  
 525  $\left(\frac{S}{Br}\right)_{\text{melt}_0}$  are the original volatile ratios in the parental (un-degassed) melt;  $D_S$ ,  $D_{Cl}$  and  $D_{Br}$   
 526 are the fluid/melt (molar) partition coefficients for the three volatiles; and  $R$  is the residual  
 527 fraction of sulfur in the melt (ranging from 1 at onset of degassing to 0 if  $S$  is totally exsolved  
 528 from the melt).

529 To resolve the model equations,  $\left(\frac{S}{Cl}\right)_{\text{melt}_0}$  and  $\left(\frac{S}{Br}\right)_{\text{melt}_0}$  are here set at 1.7 and 1320,  
 530 respectively, from the characteristic  $S$  (0.27 wt%),  $Cl$  (0.18 wt%) and  $Br$  (5.1 ppm) contents  
 531 in our most primitive, un-degassed glass inclusions from Etna (inclusion E2 from the 2001  
 532 eruption; Table A.2). The molar fluid/melt partition coefficients are obtained from our  
 533 experimental results on Etnean melts for  $Br$  ( $D_{Br}^{f/m} = 5.0$  on weight basis; Fig. 1) and those of  
 534 Alletti et al. (2009) for  $Cl$  ( $D_{Cl}^{f/m} = 8.6$  on weight basis), obtained at the same pressure (100  
 535 MPa), temperature (1200°C), redox conditions (NNO) and melt composition. These  
 536 conditions are appropriate to describe halogen behaviour in mafic magmas at shallow crustal  
 537 conditions and to extrapolate to shallow degassing, in view of the minor pressure-dependence  
 538 of halogen fluid/melt partition coefficients (Alletti et al., 2009). It is noteworthy that the  
 539 experiments of Alletti et al., (2009) were run at the low  $Cl$  concentrations (< 0.4 wt %) typical  
 540 of mafic (basaltic to andesitic) melts (Webster et al., 2009), similar to those characteristic of  
 541 the volcanoes we report gas data for in Figure 6. At such  $Cl$ -under-saturated conditions  
 542 (absence of brine formation) the minor (if any) dependence of  $D_{Cl}^{f/m}$  on total  $Cl$  contents  
 543 justifies the use of a constant  $D_{Cl}^{f/m} = 8.6$  throughout the entire degassing path. For  $S$ , a  
 544 fluid/melt partition coefficient of 86 (on weight basis) is adopted based on the results of

545 Aiuppa (2009), who found that volcanic gas measurements from Etna and several mafic arc  
546 volcanoes worldwide can satisfactorily be reproduced with a  $D_S/D_{Cl}$  ratio (ratio between  
547 fluid/melt weight partition coefficients) of 10. Our inferred  $D_S = 86$  agrees well with results  
548 obtained from S thermodynamic modelling (Moretti and Ottonello, 2005) of Etna-like melts at  
549  $P \leq 100$  MPa,  $\sim$  NNO and  $\sim 3$  wt.%  $H_2O$  (Aiuppa et al., 2007), and is within the range of  $D_S$   
550 values (3-236, by weight) obtained by Beermann et al., (2015) in their partitioning  
551 experiments between fluid and Etna-like melts at 100-200 MPa, and at either reducing or  
552 oxidizing redox conditions. We are aware that, at redox conditions close to the sulfide-sulfate  
553 transition, such as at  $\sim$  NNO (Jugo et al., 2010),  $D_S$  can exhibit large variations for even subtle  
554 redox variations (Beermann et al., 2015), and that therefore keeping  $D_S$  constant in our model  
555 is an over-simplification that does not completely reflect the real S degassing behaviour in  
556 natural (basaltic) systems. However, incorporation of such complexities (including the non-  
557 linear S partition behaviour, and its dependence on the total S content in the system;  
558 Beermann et al., 2015) into an S-Cl-Br degassing model is currently hampered by our very  
559 preliminary understanding of Br partitioning behaviour. In view of this, we find it safer to  
560 assume a constant  $D_S$  value (of 86) in our preliminary model, keeping in mind that our  
561 inferred  $D_S/D_{Cl}$  ratio is derived from empirical fitting of hundreds of volcanic gas data, and is  
562 thus likely to describe the “averaged” S degassing behaviour in mafic systems at shallow ( $\ll$   
563 3 km; Spilliaert et al., 2006) conditions relevant to halogen degassing.

564 With these numbers, and with R varied from 1 (start of degassing) to 0 (complete S exsolution  
565 from the melt), the magmatic *vapour model line* shown in Figure 6a is obtained. The evolving  
566 volatile composition of the coexisting melt is obtained by mass balance (e.g., by subtracting  
567 from the initial volatile contents, at each degassing step, the volatile fractions partitioned into  
568 the vapour phase), and is illustrated by the *melt model line* (solid red line) in Fig. 6b.

569 Our model results predict that the coexisting magmatic gas and melt (Fig. 6a, b) should both  
570 evolve with increasing degassing, from S-rich (*early gas* and *early melt*) to Cl-Br rich  
571 (relative to S) (*late gas* and *late melt*). The *vapour model line* reproduces the observed  
572 compositional range of volcanic gas samples from Etna and other mafic systems well (Fig.  
573 6a). Our calculations, therefore, provide a first, though simplistic, model to interpret Br  
574 abundance in volcanic gases from basaltic systems. We propose that high S/Br (along with  
575 S/Cl ratios; Aiuppa, 2009) gas compositions reflect shallow degassing of fertile (volatile-rich)  
576 magmas in basaltic volcano plumbing systems; while more soluble Cl and Br will prevail in  
577 gas released by later degassing stages (e.g., during near-surface syn-eruptive degassing). Our  
578 conclusions are opposite to those of Bobrowski and Giuffrida (2012) who, based on  
579 observational evidence and use of BrO gas measurements (that under-estimate total Br),  
580 proposed that low S/Br ratios mark “deep” degassing episodes of fresh basaltic magmas (at  
581 Etna). We stress, instead, that our model calculations more closely reproduce the similar  
582 *shallow* degassing behaviour of Cl and Br, which is supported by the limited variability of  
583 Cl/Br volcanic gas ratios (Fig 6a). We caution, however, that additional experimental  
584 observations, especially at low pressure, and rigorous thermodynamic models, are required to  
585 more fully constrain the fate of Br during ascent and degassing of mafic melts.

586 Our *melt model line* also suitably reproduces the compositional trends exhibited by Etna’s and  
587 Stromboli’s melt inclusions (data from Table A.2). Curiously, a set of model calculations  
588 initialised as above but with initial volatile contents from Stromboli’s most primitive  
589 inclusion (ST82c 137; S = 0.2 wt.%; Cl = 0.17 wt.%; and Br = 4.8 ppm; Table A.2) output a  
590 *melt model line* (orange line) that is very close to the Etna-like model trend above (Fig. 6b).  
591 An additional set of two model lines, calculated using slightly different initial Br contents to  
592 encompass the whole range of glass inclusion compositions observed, are also illustrated in  
593 the Figure 6b (dashed lines).

594

### 595 5.3. *Bromine contribution of volcanism to the atmosphere*

596 Global compilations show that Br sources and sinks are not strictly balanced, hinting  
597 at a missing natural source of Br (Khalil et al., 1993; Montzka et al., 2011). Methyl bromide  
598 CH<sub>3</sub>Br (mainly produced by marine phytoplankton, biomass burning and fumigants in  
599 agriculture) is the largest source of bromine to the atmosphere, and is believed to play a key  
600 role in tropospheric and stratospheric ozone depletion (e.g., Mano and Andreae, 1994;  
601 Warwick et al., 2006). However, methyl bromide alone cannot explain the total amount of  
602 active Br species involved in the ozone destruction process (e.g., Warwick et al., 2006).  
603 Following the first detection of bromine monoxide (BrO) in a volcanic plume (Bobrowski et  
604 al., 2003), volcanic degassing (both passive and active) has been recognized as a potentially  
605 major source of reactive bromine species to the atmosphere (e.g., Gerlach, 2004;  
606 Oppenheimer et al., 2006).

607 Possible approaches to quantify the volcanogenic bromine contribution to the atmosphere  
608 include: (i) direct measurements from volcanic fumaroles and plumes or (ii) calculation from  
609 bromine contents of pre-eruptive melts (i.e., undegassed crystal-hosted melt inclusions).

610 Below we apply the second approach to Etna, Merapi and Santorini volcanoes, and compare  
611 to direct gas measurements when possible.

612

#### 613 5.3.1 *Bromine emission from an open-vent mafic volcano: the case of Mount Etna*

614 Mount Etna is a persistently degassing basaltic volcano with frequent eruptive activity. We  
615 measured the Br contents of olivine-hosted melt inclusions from the trachybasaltic magma  
616 erupted during the 2006 Etna eruptions (Table A.2). This eruptive period began in mid-July  
617 2006 and continued intermittently for 5 months (Neri et al. 2006; Behncke et al., 2008); it was  
618 characterized by strombolian and effusive activity along fissures and at different vent

619 locations and by a short episode of lava fountaining (more details in Behncke et al., 2009 and  
620 references therein).

621 *Br in the pre-eruptive magma versus Br released in the atmosphere*

622 Taking into account (i) an average Br content of 5.6 ppm dissolved in the pre-eruptive melt  
623 (Table A.2), (ii) a ‘dense-rock equivalent’ (DRE) erupted volume of 0.012-0.013 km<sup>3</sup>  
624 (Supplementary Information) and (iii) 25 vol% of phenocrysts (Ferlito et al., 2010), we  
625 estimate that 125-141 tons of Br were dissolved in the melt prior to the eruption (SI).

626 The bromine output (as BrO) of this eruptive period, calculated from gas monitoring data  
627 (using an average SO<sub>2</sub> flux of 3444 tons/day, from Aiuppa et al., 2008; and a molar volcanic  
628 gas BrO/SO<sub>2</sub> ratio of  $1.1 \times 10^{-4}$ ; from Bobrowski and Giuffrida, 2012) was 85 tons. However,  
629 this is a minimum estimate since BrO is not emitted directly from the magma, but forms by  
630 conversion from HBr after emission (e.g. Oppenheimer et al 2006; Martin et al., 2009; von  
631 Glasow, 2010; Roberts et al., 2014). Thermodynamic equilibrium calculations indicate that  
632 HBr is the primary Br species at Etnean magmatic temperatures (in the 500-1100 °C  
633 temperature range and 0.1 MPa pressure; Aiuppa et al., 2005). The HBr output was  
634 unfortunately not determined during the 2006 eruption. If we assume the same mean HBr/SO<sub>2</sub>  
635 ( $7 \times 10^{-4}$  by mass) as measured in 2004 (Aiuppa et al., 2005) then this yields a Br emission of  
636 425 tons.

637 It is preferable to base the estimate on data from the actual 2006 eruption; however the  
638 percentage of BrO of the total emitted bromine is difficult to determine. BrO/SO<sub>2</sub> depends on  
639 factors including the plume age (distance from the vent, wind velocity), meteorology, time of  
640 day, etc (e.g., Bobrowski and Giuffrida, 2012). Observations and models suggest that BrO  
641 contents may represent 20 to ~50 % of total bromine within a few tens of minutes after plume  
642 release (von Glasow, 2010; Roberts et al., 2014). The total mass of bromine emitted during  
643 the 2006 Etna eruption would therefore be between 170 and 425 tons, which is comparable to

644 or larger than the mass of bromine in the pre-eruptive melt (125-141 tons, see above and SI),  
645 suggesting that Br was efficiently degassed from the basaltic melt.

#### 646 *Estimate of Br annual flux at Mount Etna*

647 On the basis of the 2006 BrO gas monitoring data encompassing non-eruptive and eruptive  
648 periods (i.e., Aiuppa et al., 2005; Bobrowski et al., 2012), we calculate a time-averaged Br  
649 emission rate of 0.7 kt/yr (assuming that BrO = 40% of Br total, Oppenheimer et al., 2006;  
650 SI). This is similar to the estimate for the 2004 eruption from Aiuppa et al. (2005). However,  
651 as highlighted by Collins et al. (2009), the 2004 and 2006 eruptions were “gas-poor  
652 eruptions” thus 0.7 kt/yr should be considered as a minimum Br annual flux for Etna.

653

#### 654 *5.3.2 Bromine emission from an andesitic volcano: the 2010 Merapi plinian eruption*

655 Merapi volcano (Java, Indonesia) is one of the most active and hazardous volcanoes in the  
656 world. The 2010 eruption (VEI 4; Solikhin et al., 2015) was the volcano’s largest since 1872.  
657 In contrast to the prolonged and effusive dome-forming eruptions typical of Merapi’s activity  
658 of the last decades, the 2010 eruption began explosively, before a new dome was rapidly  
659 emplaced. This new dome was subsequently destroyed by explosions, generating pyroclastic  
660 density currents. The initial explosive phase generated an ash plume that rose to 18 km  
661 altitude (Solikhin et al., 2015). The entire eruption released ~0.44 Tg of SO<sub>2</sub> (cumulative SO<sub>2</sub>  
662 output based on satellite observations; Surono et al., 2012), much more than previous Merapi  
663 eruptions (from 1992 to 2007; Surono et al., 2012). The SO<sub>2</sub> emission rates of the 2010  
664 eruption greatly exceed background and eruptive emissions recorded at Merapi between 1986  
665 and 2007 (Nho et al., 1996; Humaida et al., 2007; Surono et al., 2012). On the basis of the  
666 ‘petrological method’, Surono et al. (2012) and Preece et al. (2014) calculated that the magma  
667 volume needed to account for the amount SO<sub>2</sub> released is at least an order of magnitude  
668 higher than the estimated DRE volume of magma erupted. They inferred the existence of an

669 exsolved S-rich fluid phase in the pre-eruptive magma body, consistent with the conclusion  
670 given by Scaillet et al. (1998b, 2003) and Keppler (1999) to explain the common excess of  
671 sulfur upon explosive eruptions. According to VolatileCalc modelling by Preece et al. (2014),  
672 the vapour phase would have represented 1 wt% of the magma and degassing occurred in  
673 closed- (i.e., gas bubbles remained in physical contact and equilibrium with their host melt)  
674 rather than in open-system conditions prior to the explosive phase of the 2010 eruption.

675 The GOME-2 satellite instrument measured SO<sub>2</sub> SCD (slant column densities) of up to  
676  $8.9 \times 10^{18}$  molecules.cm<sup>-2</sup> (paroxysmal phase of November 5, 2010; Hormann et al., 2013),  
677 while BrO/SO<sub>2</sub> ratios were extremely low ( $8 \times 10^{-6}$  maximum), indicating that Br was virtually  
678 absent. Yet, considering a magma density of 2550 kg/m<sup>3</sup>, 55 wt% of phenocrysts (Preece et  
679 al., 2014) and an average Br content of 9 ppm in the melt inclusions (this study, Table A.2),  
680 433 tons of Br were available in the pre-eruptive melt. In addition, if we consider the presence  
681 a free fluid phase in the reservoir (1 wt%; Preece et al., 2014) and the  $D_{\text{Br}}^{\text{f/m}} = 9.1$  in andesitic  
682 melt (Fig. 2b), 73 tons of Br were stored in the fluid and hence immediately available during  
683 eruption. Note that we observe the same large discrepancy between the satellite-based  
684 estimate of the chlorine yield and the petrological one (see SI). In our opinion, the two most  
685 probable explanations are: (1) the paroxysmal phase of the eruption being ash-rich (opacity)  
686 and occurring in the middle of the night, the production of BrO was prevented until many  
687 hours later (as the reactions are UV-enabled) and is probably lower than in ash-poor plumes  
688 (2) satellite instruments measure gases which reached the stratosphere more effectively than  
689 those that remain lower in the atmosphere (significant amount of bromine might have been  
690 scavenged in the troposphere). Additional causes might include: (i) preferential S degassing  
691 owing to kinetic factors (e.g., Fiege et al., 2014), (ii) Br uptake by brine saturation during  
692 magma uprise, (iii) the involvement of other volatile species (e.g. CO<sub>2</sub>) which may alter Br  
693 partitioning.

694 The case of Merapi 2010 eruption hints at the need of studies on Br speciation in ash-rich  
695 volcanic plumes and additional experimental constraints, in particular on the effect of  
696 volatiles other than H<sub>2</sub>O on Br systematics.

697

### 698 *5.3.3. Bromine emission during the cataclysmic Minoan eruption of Santorini volcano*

699 The Late-Bronze age Minoan eruption discharged 38-86 km<sup>3</sup> DRE of rhyodacitic magma (e.g.  
700 Pyle, 1990; Johnston et al., 2014). Petrological studies have shown that the pre-eruptive melt  
701 was rich in halogens, particularly in chlorine (2500-6000 ppm), and was most probably in  
702 equilibrium with an exsolved H<sub>2</sub>O-Cl-rich fluid phase (Cadoux et al., 2014; Cadoux et al.,  
703 2015; Druitt et al., 2016). Here, we have measured for the first time the Br content of  
704 plagioclase-hosted melt inclusions from the Minoan plinian fallout deposit (Table A.2). They  
705 give an average value of  $7.3 \pm 0.8$  ppm, which multiplied by the  $D_{\text{Br}}^{\text{f/m}}$  of 20.2 (obtained in  
706 this study for a rhyodacitic composition at 900°C, 200 MPa and ~NNO; Fig. 3), indicate that  
707 the pre-eruptive fluid phase contained 147 ppm Br.

708 Assuming a minimum erupted volume of 39 km<sup>3</sup> DRE and a magma crystallinity of 10%, the  
709 Minoan pre-eruptive melt would have contained 0.6 Mt of Br. Recent studies have shown  
710 that, in silicic magma systems, Br is efficiently degassed with water during eruption (Bureau  
711 et al., 2010; Cochain et al., 2015). If we assume that all the Br was degassed from the melt  
712 (i.e. we consider 0 ppm of Br in the interstitial melt), the Br output of the Minoan eruption  
713 was 0.6 Mt. If we add the contribution of the fluid phase (assuming that it represents 5 wt% of  
714 the magma mass, as in Cadoux et al., 2015), then the total Br output would have reached 1.3  
715 Mt. These Br yields are consistent with previous estimates of 0.1-1.5 Mt (Cadoux et al., 2015)  
716 obtained by multiplying the chlorine yields by the mean molar Br/Cl ratio of 0.0022 of  
717 volcanic arc gases (Gerlach, 2004).

718 The estimated Br output of this single large explosive event (VEI 6-7) is > 100 times higher  
719 than the annual Br flux at a persistently degassing volcano such as the Etna (0.0007 Mt, see  
720 before) and the estimated global Br flux at volcanic arcs (0.005-0.015 Mt/yr; Pyle and Mather,  
721 2009).

722

## 723 **6. Conclusions**

724 Determining halogen behaviour in magmatic systems is important to understand their role in  
725 the Earth's element cycles and to provide reliable constraints on the contribution of volcanism  
726 to atmospheric and ocean chemistry. The behaviour of the heavier halogens such as Br in  
727 magmatic systems is less well understood than that of Cl and F. We have experimentally  
728 determined the fluid/melt partitioning of bromine at shallow crustal pressure and temperature  
729 conditions (100-200 MPa, 900-1200°C) with mafic, intermediate and silicic natural melts.  
730  $D_{\text{Br}}^{\text{f/m}}$  values range from  $5.0 \pm 0.3$  at 100 MPa – 1200°C for the basalt to  $20.2 \pm 1.2$  at 200  
731 MPa - 900°C for the rhyodacite. Our data confirm previous experimental constraints on  
732 synthetic model magma compositions (Bureau et al., 2000). They also show that  $D_{\text{Br}}^{\text{f/m}}$   
733 increases with increasing SiO<sub>2</sub> content of the melt (as for chlorine) and it also appears to be  
734 sensitive to melt temperature (increase of  $D_{\text{Br}}^{\text{f/m}}$  as temperature decreases). These results  
735 suggest that the Br yield into atmosphere from relatively cold and silicic magmas will be  
736 much larger than that from hotter and more mafic magmas. The partition coefficients of this  
737 study will permit better estimates of the Br yield of past explosive eruptions, provided their  
738 pre-eruptive temperature is well known.

739 Our Br partition coefficient for Etna basalt, together with literature data on S and Cl  
740 behaviour, and S-Cl-Br volcanic gas compositions in mafic volcanic systems, allow first order  
741 quantitative modelling of S-Cl-Br degassing behaviour in shallow magma reservoirs,  
742 permitting a better interpretation of gas-monitoring data.

743

## 744 **Acknowledgements**

745 A.C. thanks N. Bouden (CRPG, Nancy) for his assistance during H<sub>2</sub>O SIMS measurements,  
746 and S. Erdmann (ISTO, Orléans) who provided crystal mounts from Merapi andesite for melt  
747 inclusions analysis. A.C. is also grateful to Y. Missenard and P. Sarda (GEOPS, Orsay) for  
748 their help and discussion about error propagation. N. Metrich (IPGP, Paris) and A. Bertagnini  
749 (INGV, Pisa) provided melt inclusions from Stromboli. I. Di Carlo (ISTO, Orléans) and L.  
750 Brusca (INGV, Palermo) are acknowledged for their assistance with EMP and LA-ICPMS  
751 analyses, respectively. This work was partially supported by the ‘Laboratoire d’Excellence  
752 VOLTAIRE’ (University of Orléans, France), the French agency for research [ANR project  
753 #12-JS06-0009-01] and the European Research Council [ERC grant agreement n°305377].  
754 A.A., T.A.M. and D.M.P. acknowledge the Diamond Light Source for time on Beamline I18  
755 [Proposal sp8797]. We thank two anonymous reviewers for their insights on an earlier draft of  
756 this paper.

757

## 758 **References**

759 Aiuppa, A., 2009. Degassing of halogens from basaltic volcanism: insights from volcanic gas  
760 observations. *Chemical Geology* 263, 99-109.

761

762 Aiuppa, A., Giudice, G., Liuzzo, M., Tamburello, G., Allard, P., Calabrese, S., Chaplygin, I.,  
763 McGonigle, A.J.S. and Taran, Y. 2012, First volatile inventory for Gorely volcano,  
764 Kamchatka, *Geophys. Res. Lett.* 39, L06307

765

766 Aiuppa, A., Baker, D.R., Webster, J.D., 2009. Halogens in volcanic systems. *Chemical*  
767 *Geology* 263, 1-18.  
768

769 Aiuppa, A., Federico, C., Franco, A., Giudice, G., Gurrieri, S., Inguaggiato, S., Liuzzo, M.,  
770 McGonigle, A.J.S., Valenza, M., 2005. Emission of bromine and iodine from Mount Etna  
771 volcano. *Geochemistry, Geophysics, Geosystems* 6.  
772

773 Aiuppa, A., Federico, C., Paonita, A., Pecoraino, G., Valenza, M., 2002. S, Cl and F  
774 degassing as an indicator of volcanic dynamics: the 2001 eruption of Mount Etna. *Geophys.*  
775 *Res. Lett.* 29-11, doi 10.1029/2002GL015032.  
776

777 Aiuppa, A., Giudice, G., Gurrieri, S., Liuzzo, M., Burton, M., Caltabiano, T., McGonigle,  
778 A.J.S., Salerno, G., Shinohara, H., Valenza, M., 2008. Total volatile flux from Mount Etna.  
779 *Geophysical Research Letters* 35, L24302, doi:24310.21029/22008GL035871.  
780

781 Aiuppa, A., Moretti, R., Federico, C., Giudice, G., Gurrieri, S., Liuzzo, M., Papale, P.,  
782 Shinohara, H., Valenza, M., 2007. Forecasting Etna eruptions by real-time observation of  
783 volcanic gas composition. *Geology* 35, 1115–1118.  
784

785 Allard, P., La Spina, A., Tamburello, G., Aiuppa, A., Burton, M., Di Muro, A., Staudacher, T.  
786 (2011), First measurements of magmatic gas composition and fluxes during an eruption  
787 (October 2010) of Piton de la Fournaise hot spot volcano, La Reunion Island. Abstract, 11th  
788 Gas Workshop, Commission on the Chemistry of Volcanic Gases (CCVG)-IAVCEI-6, 2011-  
789 09 Kamchatka, Russia  
790

791 Alletti, M., 2008. Experimental investigation of halogen diffusivity and solubility in Etnean  
792 basaltic melts. University of Palermo, Palermo, Italy, p. 92.  
793

794 Alletti, M., Baker, D.R., Freda, C., 2007. Halogen diffusion in a basaltic melt. *Geochimica et*  
795 *Cosmochimica Acta* 71, 3570-3580.  
796

797 Alletti, M., Baker, D.R., Scaillet, B., Aiuppa, A., Moretti, R., Ottolini, L., 2009. Chlorine  
798 partitioning between a basaltic melt and H<sub>2</sub>O–CO<sub>2</sub> fluids at Mount Etna. *Chemical Geology*  
799 263, 37-50.  
800

801 Alletti, M., Burgisser, A., Scaillet, B., Oppenheimer, C., 2014. Chloride partitioning and  
802 solubility in hydrous phonolites from Erebus volcano: A contribution towards a multi-  
803 component degassing model. *GeoResJ* 3-4, 27-45.  
804

805 Baker, D.R., Alletti, M., 2012. Fluid saturation and volatile partitioning between melts and  
806 hydrous fluids in crustal magmatic systems: The contribution of experimental measurements  
807 and solubility models. *Earth-Science Reviews* 114, 298-324.  
808

809 Baker, D.R., Moretti, R., 2011. Modeling the Solubility of Sulfur in Magmas: A 50-Year Old  
810 Geochemical Challenge, *Reviews in Mineralogy & Geochemistry*. Mineralogical Society of  
811 America, pp. 167-213.  
812

813 Beermann, O., 2010. The solubility of sulfur and chlorine in H<sub>2</sub>O-bearing dacites of Krakatau  
814 and basalts of Mt. Etna. *Leibniz Universität Hannover, Germany, Hannover*, p. 107.  
815

816 Beermann, O., Botcharnikov, R.E., Nowak, M., 2015. Partitioning of sulfur and chlorine  
817 between aqueous fluid and basaltic melt at 1050°C, 100 and 200 MPa. *Chemical Geology*  
818 418, 132-157.

819

820 Behncke, B., Calvari, S., Giammanco, S., Neri, M., Pinkerton, H., 2008. Pyroclastic density  
821 currents resulting from interaction of basaltic magma with hydrothermally altered rock: An  
822 example from the 2006 summit eruptions of Mount Etna (Italy). *Bull. Volcanol.* 70, 1249–  
823 1268, doi:1210.1007/s00445-00008-00200-00447.

824

825 Behncke, B., Falsaperla, S., Pecora, E., 2009. Complex magma dynamics at Mount Etna  
826 revealed by seismic, thermal and volcanological data. *J. Geophys. Res.* 114, B03211,  
827 doi:03210.01029/02008JB005882.

828

829 Bobrowski, N., Giuffrida, G., 2012. Bromine monoxide / sulphur dioxide ratios in relation to  
830 volcanological observations at Mt. Etna 2006-2009. *Solid Earth* 3, 433-445.

831

832 Bobrowski, N., Hönninger, G., Galle, B., Platt, U., 2003. Detection of bromine monoxide in a  
833 volcanic plume. *Nature* 423, 273–276.

834

835 Bobrowski, N., von Glasow, R., Giuffrida, G.B., Tedesco, D., Aiuppa, A., Yalire, M.,  
836 Arellano, S., Johansson, M., Galle, B., 2015. Gas emission strength and evolution of the  
837 molar ratio of BrO/SO<sub>2</sub> in the plume of Nyiragongo in comparison to Etna. *Journal of*  
838 *Geophysical Research: Atmospheres* 120, 277-291.

839

840 Borodulin, G.P., Chevychelov, V.Y., Zaraysky, G.P., 2009. Experimental study of  
841 partitioning of tantalum, niobium, manganese, and fluorine between aqueous fluoride fluid  
842 and granitic and alkaline melts. *Doklady Earth Sciences* 427, 868-873.  
843

844 Botcharnikov, R.E., Behrens, H., Holtz, F., Koepke, J., Sato, H., 2004. Sulfur and chlorine  
845 solubility in Mt. Unzen rhyodacitic melt at 850°C and 200 MPa. *Chem Geol* 213, 207-225.  
846

847 Botcharnikov, R.E., Holtz, F., Behrens, H., 2007. The effect of CO<sub>2</sub> on the solubility of H<sub>2</sub>O-  
848 Cl fluids in andesitic melt. *Eur J Mineral* 19, 671-680.  
849

850 Botcharnikov, R.E., Holtz, F., Behrens, H., 2015. Solubility and fluid-melt partitioning of  
851 H<sub>2</sub>O and Cl in andesitic magmas as a function of pressure between 50 and 500 MPa. *Chem*  
852 *Geol*, doi:10.1016/j.chemgeo.2015.1007.1019.  
853

854 Bureau, H., Auzende, A.L., Marocchi, M., Raepsaet, C., Munsch, P., Testemale, D., Mézouar,  
855 M., Kubsky, S., Carrière, M., Ricolleau, A., Fiquet, G., 2016. Modern and past volcanic  
856 degassing of iodine. *Geochimica et Cosmochimica Acta* 173, 114-125.  
857

858 Bureau, H., Foy, E., Raepsaet, C., Somogyi, A., Munsch, P., Simon, G., Kubsky, S., 2010.  
859 Bromine cycle in subduction zones through in situ Br monitoring in diamond anvil cells.  
860 *Geochimica et Cosmochimica Acta* 74, 3839-3850.  
861

862 Bureau, H., Keppler, H., Métrich, N., 2000. Volcanic degassing of bromine and iodine:  
863 experimental fluid/melt partitioning data and applications to stratospheric chemistry. *Earth*  
864 *and Planetary Science Letters* 183, 51-60.

865

866 Bureau, H., Métrich, N., 2003. An experimental study of bromine behaviour in water-  
867 saturated silicic melts. *Geochimica et Cosmochimica Acta* 67, 1689-1697.

868

869 Cadoux, A., Iacono-Marziano, G., Paonita, A., Deloule, E., Aiuppa, A., Eby, G.N., Costa, M.,  
870 Brusca, L., Berlo, K., Geraki, K., Mather, T.A., Pyle, D.M., Di Carlo, I., 2017. A new set of  
871 standards for in-situ measurement of bromine abundances in natural silicate glasses:  
872 application to SR-XRF, LA-ICP-MS and SIMS techniques. *Chemical Geology* 452, 60-70.

873

874 Cadoux, A., Scaillet, B., Bekki, S., Oppenheimer, C., Druitt, T.H., 2015. Stratospheric Ozone  
875 destruction by the Bronze-Age Minoan eruption (Santorini Volcano, Greece). *Scientific*  
876 *Reports* 5, 12243.

877

878 Cadoux, A., Scaillet, B., Druitt, T.H., Deloule, E., 2014. Magma storage conditions of large  
879 Plinian eruptions of Santorini Volcano (Greece). *Journal of Petrology* 55, 1129-1171.

880

881 Carroll, M.R., Webster, J.D., 1994. Solubilities of sulfur, noble gases, nitrogen, chlorine, and  
882 fluorine in magmas, in: Carroll, M.R., Holloway, J.R. (Eds.), *Volatiles in Magmas*.  
883 *Mineralogical Society of America*, pp. 231-279.

884

885 Chevychelov, V.Y., Bocharnikov, R.E., Holtz, F., 2008a. Experimental study of chlorine and  
886 fluorine partitioning between fluid and subalkaline basaltic melt. *Doklady Earth Sciences* 422,  
887 1089–1092.

888

889 Chevychelov, V.Y., Botcharnikov, R.E., Holtz, F., 2008b. Partitioning of Cl and F between  
890 fluid and hydrous phonolitic melt of Mt. Vesuvius at 850-1000 °C and 200 MPa. *Chem. Geol.*  
891 256, 172–184.

892

893 Cochain, B., Sanloup, C., de Grouchy, C., Crépisson, C., Bureau, H., Leroy, C., Kantor, I.,  
894 Irifune, T., 2015. Bromine speciation in hydrous silicate melts at high pressure. *Chemical*  
895 *Geology* 404, 18-26.

896

897 Collins, S.J., Pyle, D.M., Maclennan, J., 2009. Melt inclusions track pre-eruption storage and  
898 dehydration of magmas at Etna. *Geology* 37, 571–574.

899

900 Costa, F., Andreastuti, S., Bouvet de Maisonneuve, C., Pallister, J.S., 2013. Petrological  
901 insights into the storage conditions, and magmatic processes that yielded the centennial 2010  
902 Merapi explosive eruption. *Journal of Volcanology and Geothermal Research* 261, 209-235.

903

904 Daniel, J.S., Solomon, S., Portmann, R.W., Garcia, R.R., 1999. Stratospheric ozone  
905 destruction: The importance of bromine relative to chlorine. *J. Geophys. Res.* 104, 23871–  
906 23880.

907

908 de Chambost, E., Schumacher, M., Lovestam, G., Claesson, S., 1996. Achieving high  
909 transmission with the Cameca IMS 1270, in: Benninghoven, A., Hagenhoff, B., Werner, H.W.  
910 (Eds.), *Secondary Ion Mass Spectrometry, SIMS X*. Wiley, Chichester, pp. 1003-1006.

911

912 Di Carlo, I., Pichavant, M., Rotolo, S.G., Scaillet, B., 2006. Experimental crystallization of a  
913 high-K arc basalt: the golden pumice, Stromboli volcano (Italy). *Journal of Petrology* 47,  
914 1317-1343.

915

916 Dolejs, D., Baker, D.R., 2007a. Liquidus equilibria in the system  $K_2O-Na_2O-Al_2O_3-SiO_2-$   
917  $F_2O-H_2O$  to 100 MPa: I. Silicate fluoride liquid immiscibility in anhydrous systems. *J*  
918 *Petrol* 48, 785-806.

919

920 Dolejs, D., Baker, D.R., 2007b. Liquidus equilibria in the system  $K_2O-Na_2O-Al_2O_3-SiO_2-$   
921  $F_2O-H_2O$  to 100 MPa: II. Differentiation paths of fluorosilicic magmas in hydrous  
922 systems. *J Petrol* 48, 807-828.

923

924 Druitt, T.H., Mercier, M., Florentin, L., Deloule, E., Cluzel, N., Flaherty, T., Médard, E.,  
925 Cadoux, A., 2016. Magma Storage and Extraction Associated with Plinian and Interplinian  
926 Activity at Santorini Caldera (Greece). *Journal of Petrology* 57, 461-494.

927

928 Edmonds, M., Gerlach, T.M., Herd, R.A., 2009. Halogen degassing during ascent and  
929 eruption of water-poor basaltic magma. *Chemical Geology* 263, 122-130.

930

931 Ferlito, C., Viccaro, M., Nicotra, E., Cristofolini, R., 2010. Relationship between the flank  
932 sliding of the South East Crater (Mt. Etna, Italy) and the paroxysmal event of November 16,  
933 2006. *Bulletin of Volcanology* 72, 1179-1190.

934

935 Fiege, A., Behrens, H., Holtz, F. and Adams, F. (2014) Kinetic vs. thermodynamic control of  
936 degassing of  $H_2O-S\pm Cl$ -bearing andesitic melts. *Geochim. Cosmochim. Acta* 125, 241-264.

937 Foustoukos, D.I., Seyfried, W.E., 2007. Trace element partitioning between vapor, brine and  
938 halite under extreme phase separation conditions. *Geochim. Cosmochim. Acta* 71, 2056–  
939 2071.

940

941 Gaillard, F., Scaillet, B., 2014. A theoretical framework for volcanic degassing chemistry in a  
942 comparative planetology perspective and implications for planetary atmospheres. *Earth and  
943 Planetary Science Letters* 403, 307-316.

944

945 Gennaro M.E. (2017). Sulfur behavior and redox conditions in Etnean hydrous basalts  
946 inferred from melt inclusions and experimental glasses. PhD thesis. Università degli Studi di  
947 Palermo.

948

949 Gerlach, T.M., 2004. Volcanic sources of tropospheric ozone-depleting trace gases.  
950 *Geochemistry, Geophysics, Geosystems* 5, Q09007.

951

952 Hörmann, C., Sihler, H., Bobrowski, N., Beirle, S., Penning de Vries, M., Platt, U., Wagner,  
953 T., 2013. Systematic investigation of bromine monoxide in volcanic plumes from space by  
954 using the GOME-2 instrument. *Atmos. Chem. Phys.* 13, 4749-4781.

955

956 Humaida, H., Sumarti, S., Subandriyo, Nandaka, A., Sukarnen, I.G.M., Suharno, Rinekso, K.,  
957 Badrijas, Ismai, Sunarto, 2007. Aktivitas Merapi 2006 dan Pemantauan Emisi SO<sub>2</sub> dengan  
958 COSPEC, in *Erupsi Merapi 2006. Laporan dan Kajian Vulkanisme Erupsi 2006*. Departement  
959 Energi dan Sumber Daya Mineral, Badan Geologi, Pusat Vulkanologi dan Mitigasi Bencana  
960 Geologi.

961

962 Iacono-Marziano, G., Morizet, Y., Le Trong, E., Gaillard, F., 2012. New experimental data  
963 and semi-empirical parameterization of H<sub>2</sub> O-CO<sub>2</sub> solubility in mafic melts. *Geochimica et*  
964 *Cosmochimica Acta* 97, 1-23.

965

966 Johnston, E.N., Sparks, R.S.J., Phillips, J.C., Carey, S., 2014. Revised estimates for the  
967 volume of the late Bronze Age Minoan eruption, Santorini. *Journal of the Geological Society,*  
968 *London*, 171, 583-590.

969

970 Jugo, P.J., Wilke, M., Botcharnikov, R.E., 2010. Sulfur K-edge XANES analysis of natural  
971 and synthetic basaltic glasses: implications for S-speciation and S content as function of  
972 oxygen fugacity. *Geochim. Cosmochim. Acta* 74, 5926–5938.

973

974 Kahl, M., Chakraborty, S., Pompilio, M., Costa, F., 2015. Constraints on the Nature and  
975 Evolution of the Magma Plumbing System of Mt. Etna Volcano (1991-2008) from a  
976 Combined Thermodynamic and Kinetic Modelling of the Compositional Record of Minerals.  
977 *Journal of Petrology* 56, 2025-2068.

978

979 Kendrick, M.A., Arculus, R.J., Danyushevsky, L.V., Kamenetsky, V.S., Woodhead, J.D.,  
980 Honda, M., 2014. Subduction-related halogens (Cl, Br and I) and H<sub>2</sub>O in magmatic glasses  
981 from Southwest Pacific Backarc Basins. *Earth and Planetary Science Letters* 400, 165-176.

982

983 Keppler, H. (1999) Experimental Evidence for the Source of Excess Sulfur in Explosive  
984 Volcanic Eruptions. *Science* 284, 1652-1654.

985

986 Khalil, M.A.K., Rasmussen, R.A., Gunawardena, R., 1993. Atmospheric methyl bromide:  
987 Trends and global mass balance. *Journal of Geophysical Research: Atmospheres* 98, 2887-  
988 2896.

989

990 Kutterolf, S., Hansteen, T.H., Appel, K., Freundt, A., Krüger, K., Pérez, W., Wehrmann, H.,  
991 2013. Combined bromine and chlorine release from large explosive volcanic eruptions: A  
992 threat to stratospheric ozone? *Geology* 41, 707–710.

993

994 Lesne, P., Scaillet, B., Pichavant, M., 2015. The solubility of sulfur in hydrous basaltic melts.  
995 *Chemical Geology* 418, 104-116.

996

997 Lesne, P., Scaillet, B., Pichavant, M., Beny, J.-M., 2011b. The carbon dioxide solubility in  
998 alkali basalts: an experimental study. *Contributions to Mineralogy and Petrology* 162, 153-  
999 168.

1000

1001 Lesne, P., Scaillet, B., Pichavant, M., Iacono-Marziano, G., Beny, J.-M., 2011a. The H<sub>2</sub> O  
1002 solubility of alkali basaltic melts: an experimental study. *Contributions to Mineralogy and*  
1003 *Petrology* 162, 133-151.

1004

1005 Longerich, H.P., Jackson, S.E., Fryer, B.J., Strong, D.F., 1993. The laser ablation microprobe  
1006 inductively coupled plasma-mass spectrometer. *Geoscience Canada* 20, 21-27.

1007

1008 Manó, S., Andreae, M.O., 1994. Emission of Methyl Bromide from Biomass Burning.  
1009 *Science* 263, 1255.

1010

1011 Martel, C., Pichavant, M., Holtz, F., Scaillet, B., Bourdier, J.-L., Traineau, H., 1999. Effects  
1012 of  $fO_2$  and  $H_2O$  on andesite phase relations between 2 and 4 kbar. *J. Geophys. Res.* 104,  
1013 29,453–429,470.

1014

1015 Martin, R.S., Roberts, T.J., Mather, T.A., Pyle, D.M., 2009. The implications of  $H_2S$  and  $H_2$   
1016 stability in high-T mixtures of magmatic and atmospheric gases for the production of oxidized  
1017 trace species (e.g., BrO and NO<sub>x</sub>). *Chem. Geol.* 263, 143–150.

1018

1019 Mather, T.A., 2015. Volcanoes and the environment: Lessons for understanding Earth's past  
1020 and future from studies of present-day volcanic emissions. *Journal of Volcanology and*  
1021 *Geothermal Research* 304, 160-179.

1022

1023 Mather, T.A., Witt, M.L.I., Pyle, D.M., Quayle, B.M., Aiuppa, A., Bagnato, E., Martin, R.S.,  
1024 Sims, K.W.W., Edmonds, M., Sutton, A.J., Ilyinskaya, E., 2012. Halogens and trace metal  
1025 emissions from the ongoing 2008 summit eruption of Kīlauea volcano, Hawaii *Geochimica et*  
1026 *Cosmochimica Acta* 83, 292-323.

1027

1028 Métrich, N., Allard, P., Spilliarde, N., Andronico, D., Burton, M., 2004. 2001 flank eruption  
1029 of the alkali- and volatile-rich primitive basalt responsible for Mount Etna's evolution in the  
1030 last three decades. *Earth and Planetary Science Letters* 228, 1–17.

1031

1032 Métrich, N., Bertagnini, A., Di Muro, A., 2010. Conditions of magma storage, degassing and  
1033 ascent at Stromboli: new insights into the volcano plumbing system with inferences on the  
1034 eruptive dynamics. *J. Petrol.* 51, 603-626.

1035

1036 Métrich, N., Bertagnini, A., Landi, P., Rosi, M., 2001. Crystallisation driven by  
1037 decompression and water loss at Stromboli volcano (Aeolian Islands). *J. Petrol.* 42, 1471-  
1038 1490.

1039

1040 Métrich, N., Deloule, E., 2014. Water content,  $\delta D$  and  $\delta^{11}B$  tracking in the Vanuatu arc  
1041 magmas (Aoba Island): Insights from olivine-hosted melt inclusions. *Lithos* 206-207, 400-  
1042 408.

1043

1044 Métrich, N., Wallace, P., 2008. Volatile abundances in basaltic magmas and their degassing  
1045 paths tracked by melt inclusions, in: Putirka, K., Tepley, F. (Eds.), *Minerals, Inclusions and*  
1046 *Volcanic Processes*. Mineralogical Society of America, pp. 363-402.

1047

1048 Montzka, S., and Reimann, S. (Coordinating Lead Authors), Engel, A., Krüger, K.,  
1049 O'Doherty, S., Sturges, W.T., Blake, D., Dorf, M., Fraser, P., Froidevaux, L., Jucks, K.,  
1050 Kreher, K., Kurylo, M.J., Mellouki, A., Miller, J., Nielsen, O.-J., Orkin, V.L., Prinn, R.G.,  
1051 Rhew, R., Santee, M.L., Stohl, A., and Verdonik, D., Ozone-depleting substances (ODSs) and  
1052 related chemicals, Chapter 1 in *Scientific Assessment of Ozone Depletion: 2010*, Global  
1053 Ozone Research and Monitoring Project–Report No. 52, 516 pp., World Meteorological  
1054 Organization, Geneva, Switzerland, 2011.

1055

1056 Moretti, R., Ottonello, G., 2005. Solubility and speciation of sulfur in silicate melts: The  
1057 Conjugated Toop-Samis-Flood-Grjotheim (CTSFG) model. *Geochimica et Cosmochimica*  
1058 *Acta* 69, 801-823.

1059

1060 Mungall, J.E. and Brenan, J.M. (2003) Experimental evidence for the chalcophile behavior of  
1061 the halogens. *Can. Mineral.* 41, 207-220.

1062

1063 Neri, M., Behncke, B., Burton, M., Galli, G., Giammanco, S., Pecora, E., Privitera, E.,  
1064 Reitano, D., 2006. Continuous soil radon monitoring during the July 2006 Etna eruption.  
1065 *Geophys. Res. Lett.* 33, L24316, doi: 24310.21029/22006GL028394.

1066

1067 Nho, E.-Y., Le Cloarec, M.-F., Ardouin, B., Tjetjep, W.S., 1996. Source strength assessment  
1068 of volcanic trace elements emitted from the Indonesian Arc. *Journal of Volcanology and*  
1069 *Geothermal Research* 74, 121–129.

1070

1071 Oppenheimer, C., Tsanev, V.I., Braban, C.F., Cox, R.A., Adams, J.W., Aiuppa, A.,  
1072 Bobrowski, N., Delmelle, P., Barclay, J., McGonigle, A.J.S., 2006. BrO formation in volcanic  
1073 plumes. *Geochimica et Cosmochimica Acta* 70, 2935-2941.

1074

1075 Preece, K., Gertisser, R., Barclay, J., Berlo, K., Herd, R.A., 2014. Pre- and syn-eruptive  
1076 degassing and crystallisation processes of the 2010 and 2006 eruptions of Merapi volcano,  
1077 Indonesia. *Contributions to Mineralogy and Petrology* 168, 1061.

1078

1079 Pyle, D.M., 1990, New volume estimates for the Minoan eruption, In: *Thera and the Aegean*  
1080 *World III*, vol 2, eds. D Hardy, J. Keller, VP Galanopoulos, NC Flemming and TH Druitt, pp  
1081 113-121; The Thera Foundation, London.

1082

1083 Pyle, D.M., Mather, T.A., 2009. Halogens in igneous processes and their fluxes to the  
1084 atmosphere and oceans from volcanic activity: A review. *Chemical Geology* 263, 110-121.

1085

1086 Kravchuk, F., Keppler, H., 1994. Distribution of chloride between aqueous fluids and felsic  
1087 melts at 2 kbar and 800°C. *Eur. J. Mineral.* 6, 913-923.

1088

1089 Roberts, T.J., Braban, C.F., Martin, R.S., Oppenheimer, C., Adams, J.W., Cox, R.A.,  
1090 Griffiths, P.T., 2009. Modelling reactive halogen formation and ozone depletion in volcanic  
1091 plumes. *Chemical Geology* 263, 151-163.

1092

1093 Roberts, T.J., Martin, R.S., Jourdain, L., 2014. Reactive bromine chemistry in Mount Etna's  
1094 volcanic plume: the influence of total Br, high-temperature processing, aerosol loading and  
1095 plume–air mixing. *Atmospheric Chemistry and Physics* 14, 11201-11219.

1096

1097 Sawyer, G.M., Salerno, G.G., Le Blond, J.S., Martin, R.S., Spampinato, L., Roberts, T.J.,  
1098 Mather, T.A., Witt, M.L.I., Tsanev, V.I. and Oppenheimer, C. 2011, Gas and aerosol  
1099 emissions from Villarrica volcano, Chile, *J. Volcanol. Geotherm. Res.* 203, 62-75.

1100

1101 Scaillet, B., Holtz, F., Pichavant, M., 1998a. Phase equilibrium constraints on the viscosity of  
1102 silicic magmas: 1. Volcanic-plutonic comparison. *Journal of Geophysical Research: Solid*  
1103 *Earth* 103, 27257-27266.

1104

1105 Scaillet, B., Clémente, B., Evans, B. W., & Pichavant, M. 1998b. Redox control of sulfur  
1106 degassing in silicic magmas. *Journal of Geophysical Research: Solid Earth*, 103(B10),  
1107 23937-23949.

1108

1109 Scaillet, B., Evans, B.W., 1999. The 15 June 1991 Eruption of Mount Pinatubo. I. Phase  
1110 Equilibria and Pre-eruption P-T-f O<sub>2</sub> -f H<sub>2</sub> O Conditions of the Dacite Magma. Journal of  
1111 Petrology 40, 381-411.  
1112  
1113 Scaillet, B., Luhr, J. F., & Carroll, M. R. 2003. Petrological and volcanological constraints on  
1114 volcanic sulfur emissions to the atmosphere. *Volcanism and the Earth's Atmosphere*, AGU  
1115 Monograph 139, 11-40.  
1116  
1117 Seo, J.H., Zajacz, Z., 2016. Fractionation of Cl/Br during fluid phase separation in magmatic–  
1118 hydrothermal fluids. *Geochim. Cosmochim. Acta* 183, 125–137.  
1119  
1120 Shannon, R.D., 1976. Revised effective ionic radii and systematic studies of interatomic  
1121 distances in halides and chalcogenides. *Acta Cryst. A* 32, 751-767.  
1122  
1123 Shishkina, T.A., Botcharnikov, R.E., Holtz, F., Almeev, R.R., Portnyagin, M.V., 2010.  
1124 Solubility of H<sub>2</sub> O- and CO<sub>2</sub> -bearing fluids in tholeiitic basalts at pressures up to 500 MPa.  
1125 *Chemical Geology* 277, 115-125.  
1126  
1127 Signorelli, S., Carroll, M.R., 2000. Solubility and fluid-melt partitioning of Cl in hydrous  
1128 phonolitic melts. *Geochimica et Cosmochimica Acta* 64, 2851-2862.  
1129  
1130 Solikhin, A., Thouret, J.-C., Liew, S.C., Gupta, A., Sayudi, D.S., Oehler, J.-F., Kassouk, Z.,  
1131 2015. High-spatial-resolution imagery helps map deposits of the large (VEI 4) 2010 Merapi  
1132 Volcano eruption and their impact. *Bulletin of Volcanology* 77, 20.  
1133

1134 Spilliaert, N., Metrich, N., Allard, P., 2006. S-Cl-F degassing pattern of water rich alkali  
1135 basalt: modelling and relationship with eruption styles of Mount Etna volcano. *Earth Planet.*  
1136 *Sci. Lett.* 248, 772-786.

1137

1138 Stelling, J., Botcharnikov, R.E., Beermann, O., Nowak, M., 2008. Solubility of H<sub>2</sub>O- and  
1139 chlorine-bearing fluids in basaltic melt of Mount Etna at T = 1050-1205°C and P = 200 MPa.  
1140 *Chemical Geology* 256, 102-110.

1141

1142 Surono, Jousset, P., Pallister, J., Boichu, M., Buongiorno, M.F., Budisantoso, A., Costa, F.,  
1143 Andreastuti, S., Prata, F., Schneider, D., Clarisse, L., Humaida, H., Sumarti, S., Bignami, C.,  
1144 Griswold, J., Carn, S., Oppenheimer, C., Lavigne, F., 2012. The 2010 explosive eruption of  
1145 Java's Merapi volcano - A '100-year' event. *Journal of Volcanology and Geothermal Research*  
1146 241-242, 121-135.

1147

1148 von Glasow, R., 2010. Atmospheric chemistry in volcanic plumes. *Proceedings of the*  
1149 *National Academy of Sciences* 107, 6594-6599, doi:6510.1073/pnas.0913164107.

1150

1151 von Glasow, R., Bobrowski, N., Kern, C., 2009. The effects of volcanic eruptions on  
1152 atmospheric chemistry. *Chemical Geology* 263, 131-142.

1153

1154 Warwick, N.J., Pyle, J.A., Carver, G.D., Yang, X., Savage, N.H., O'Connor, F.M., Cox, R.A.,  
1155 2006. Global modeling of biogenic bromocarbons. *J. Geophys. Res.* 111, D24305,  
1156 doi:24310.21029/22006JD007264.

1157

1158 Webster, J.D., 1990. Partitioning of F between H<sub>2</sub>O and CO<sub>2</sub> fluids and topaz rhyolite melt.  
1159 Contrib Mineral Petrol 104, 424-438.  
1160  
1161 Webster, J.D., 1992a. Water solubility and chlorine partitioning in Cl-rich granitic systems:  
1162 Effects of melt composition at 2 kbar and 800°C. *Geochimica et Cosmochimica Acta* 56, 679-  
1163 687.  
1164  
1165 Webster, J.D., 1992b. Fluid–melt interactions involving Cl-rich granites: experimental study  
1166 from 2 to 8 kbar. *Geochimica et Cosmochimica Acta* 56, 679–687.  
1167  
1168 Webster, J.D., 2004. The exsolution of magmatic hydrosaline melts. *Chem Geol* 210, 33-48.  
1169  
1170 Webster, J.D., Holloway, J.R., 1990. Partitioning of F and Cl between hydrothermal fluids  
1171 and highly evolved granitic magmas, in: Stein, H.J., Hannah, J.L. (Eds.), *Ore-bearing granite*  
1172 *systems: Petrogenesis and mineralizing processes*. Geological Society of America Special  
1173 Paper, pp. 21-34.  
1174  
1175 Webster, J.D., Kinzler, R.J., Mathez, E.A., 1999. Chloride and water solubility in basalt and  
1176 andesite melts and implications for magmatic degassing. *Geochimica et Cosmochimica Acta*  
1177 63, 729-738.  
1178  
1179 Webster, J.D., De Vivo, B., Tappen, C., 2003. Volatiles, magmatic degassing and eruptions of  
1180 Mt. Somma-Vesuvius: constraints from silicate melt inclusions, solubility experiments and  
1181 modeling, in: De Vivo, B., Bodnar, R.J. (Eds.), *Melt Inclusions in Volcanic Systems:*  
1182 *Methods, Applications and Problems*. Dev Volcanol Elsevier, Amsterdam, pp. 207-226.

1183

1184 Webster, J.D., Tappen, C.M., Mandeville, C.W., 2009. Partitioning behavior of chlorine and  
1185 fluorine in the system apatite-melt-fluid. II: Felsic silicate systems at 200 MPa. *Geochimica et*  
1186 *Cosmochimica Acta* 73, 559-581.

1187

1188 Webster, J.D., Goldoff, B., Sintoni, M.F., Shimizu, N., De Vivo, B., 2014. C-O-H-Cl-S-F  
1189 volatile solubilities, partitioning, and mixing in phonolitic-trachytic melts and aqueous-  
1190 carbonic vapor ± saline liquid at 200 MPa. *J Petrol* 55, 2217-2248.

1191

1192 Webster, J.D., Vetere, F., Botcharnikov, R.E., Goldoff, B., McBirney, A., Doherty, A.L.,  
1193 2015. Experimental and modeled chlorine solubilities in aluminosilicate melts at 1 to 7000  
1194 bars and 700 to 1250 °C: Applications to magmas of Augustine Volcano, Alaska. *American*  
1195 *Mineralogist* 100, 522-535.

1196

1197 Webster, J.D., Baker, D.R., Aiuppa, A., 2018. Halogens in Mafic and Intermediate-silica  
1198 Content Magmas, in: Harlow, D., Aranovich, L.Y. (Eds.), *The Role of Halogens in Terrestrial*  
1199 *and Extraterrestrial Geochemical Processes: Surface, Crust, and Mantle*. Springer  
1200 International Publishing, pp. VI, 1030.

1201

1202 Witt, M. L. I., T. A. Mather, D. M. Pyle, A Aiuppa, E. Bagnato, and V. I. Tsanev (2008),  
1203 Mercury and halogen emissions from Masaya and Telica volcanoes, Nicaragua, *J. Geophys.*  
1204 *Res.*, 113, B06203, doi:10.1029/2007JB005401

1205

1206 Zajacz, Z., Candela, P.A., Piccoli, P.M., Sanchez-Valle, C., 2012. The partitioning of sulfur  
1207 and chlorine between andesite melts and magmatic volatiles and the exchange coefficients of  
1208 major cations. *Geochim Cosmochim Acta* 89, 81-101.

1209 **Figure Captions**

1210

1211 **Figure 1.** Partitioning of bromine between melt and fluid in the run products at 1200°C, 100  
1212 MPa and  $fO_2 \sim NNO$ . The  $D_{Br}^{f/m}$  of the basaltic composition, determined by linear regression  
1213 through the origin, is:  $4.95 \pm 0.33$ . The error on the partition coefficient corresponds to the  
1214 error on the slope of the regression line, as determined by the least squares method.

1215

1216 **Figure 2. (a)** Melt Br contents versus bulk Br contents (ppm) for the andesitic and rhyodacitic  
1217 compositions at 1060°C, 200 MPa and  $fO_2 \sim NNO$ . **(b)** and **(c)** Partitioning of bromine  
1218 between melt and fluid in the andesitic and rhyolitic run products, respectively, at those  
1219 conditions. The  $D_{Br}^{f/m}$  determined by linear regression through the origin are:  $9.1 \pm 0.6$  for the  
1220 andesite and  $14.0 \pm 0.6$  for the rhyodacite. The errors on  $D_{Br}^{f/m}$  are the errors on the regression  
1221 lines slope, see Figure 1 caption.

1222

1223 **Figure 3.** Partitioning of bromine between melt and fluid for the rhyodacitic composition, at  
1224 900°C, 200 MPa,  $\sim NNO$ . At lower temperature, the  $D_{Br}^{f/m}$  of the rhyodacite increases:  $20.2 \pm$   
1225  $1.2$ . Error on  $D_{Br}^{f/m}$ : see Figure 1 caption. The results are consistent with those of Bureau et al.  
1226 (2000) on synthetic albite composition.

1227

1228 **Figure 4.**  $D_{Br}^{f/m}$  as a function of  $SiO_2$  (wt%) of the run products of this study. The data for the  
1229 900°C – 200 MPa experiment of Bureau et al. (2000) is also plotted. This figure shows the  
1230 effect of melt composition on  $D_{Br}^{f/m}$  and also suggests an effect of the temperature, at least for  
1231 the more silicic melts.

1232

1233 **Figure 5.**  $D_{\text{Br}}^{f/m}$  of the rhyodacite composition versus partition experiment temperature (°C).

1234 Data at 900°C and 1060°C are at 200 MPa and data at 1200°C is at 100 MPa.

1235

1236 **Figure 6. (a)** Triangular plot of S-Cl-Br\*300 compositions of volcanic gas samples from  
1237 selected mafic arc volcanoes. All data refer to near-vent in-situ measurements with filter  
1238 packs, and are thus representative of gas species SO<sub>2</sub>, HCl and HBr (the main S and halogen  
1239 reservoirs in near-vent plumes, Aiuppa et al., 2005). Volcanic gas data sources: Reunion  
1240 Island (Indian Ocean): Allard et al (2011); Nyiragongo (Congo): Bobrowski et al. (2015);  
1241 Hawaii (Pacific Ocean): Mather et al., (2012); Etna (Sicily): Aiuppa et al. (2005), Aiuppa,  
1242 (2009), Aiuppa, unpublished results; Stromboli (Aeolian Islands): Aiuppa, (2009); Masaya  
1243 (Nicaragua): Witt et al, (2008); Mount Asama (Japan): Aiuppa, (2009), Aiuppa, unpublished  
1244 results; Myike-jima (Japan): Aiuppa, (2009), Aiuppa, unpublished results; Gorely  
1245 (Kamchatka, Russia): Aiuppa et al. (2012); Villarrica (Chile): Sawyer et al., (2011). For  
1246 comparison, the model-derived compositions of gas initially coexisting with an Etna-like  
1247 primitive melt (S: 0.27 wt.%, Cl: 0.18 wt.%, and Br: 5.1 ppm) are shown by the thick solid  
1248 green curve. Dashed green lines are examples of Etna-like melt model trends obtained using  
1249 same initial S and Cl contents (S: 0.27 wt.%, Cl: 0.18 wt.%) but slightly different initial Br  
1250 contents (of respectively 3 and 6.1 ppm), within the range observed in glass inclusions (see  
1251 Table A.2). The initial Br contents for the 3 Etna runs are labeled in the plot. Model lines are  
1252 obtained using the Rayleigh-type open-system equations described in the text. Extent of  
1253 degassing along both model lines varies from top (“early gas”) to bottom (“late gas”) (R  
1254 values for specific points are shown in italics). See text for discussion. **(b)** The glass inclusion  
1255 compositions from Etna and Stromboli (data from Table A.2) are displayed against the model-  
1256 derived compositions, ranging from S-rich “*early melts*” to halogen-enriched (relative to S)  
1257 “*late melts*”. The melt model line (solid red curve) is derived from the same Etna-like

1258 primitive melt composition given above (S: 0.27 wt.%, Cl: 0.18 wt.%, and Br: 5.1 ppm).  
1259 Dashed red lines are examples of Etna-like melt model trends obtained using same initial S  
1260 and Cl contents (S: 0.27 wt.%, Cl: 0.18 wt.%) but slightly different initial Br contents (of  
1261 respectively 3 and 6.1 ppm), within the range observed in glass inclusions (see Table A.2).  
1262 The initial Br contents for the 3 Etna runs are labeled in the plot. The melt model trend  
1263 initialized at conditions representative of a Stromboli's primitive melt (S: 0.2 wt.%, Cl: 0.17  
1264 wt.%, and Br: 4.8 ppm; see Table A.2) is depicted by the orange solid line. R values for  
1265 specific points are shown in italics.

1266

1267 **Table Captions**

1268

1269 **Table 1.** Major element composition of the starting dry glasses used for the partitioning  
1270 experiments.

1271

1272 **Table 2.** Results of the fluid/melt partitioning experiments.

1273

1274 **Table 3.** Major element composition (wt%) of the partition experiment products.

**Table 1.** Major element composition of the starting dry glasses used for the partitioning experiments

<b>Volcano: Eruption</b>	<b>Etna: 11/22/2002</b>		<b>Santorini: USC-2</b>		<b>Santorini: Minoan</b>	
Sample name	ET02PA27 <sup>a</sup>		S09-22 <sup>b</sup>		S82-30 <sup>c</sup>	
<i>Major oxides (wt%)</i>	<i>n = 32</i>	$\pm 1\sigma$	<i>n = 8</i>	$\pm 1\sigma$	<i>n = 22</i>	$\pm 1\sigma$
SiO <sub>2</sub>	47.95	0.82	58.88	0.43	71.24	0.26
TiO <sub>2</sub>	1.67	0.11	1.28	0.05	0.45	0.04
Al <sub>2</sub> O <sub>3</sub>	17.32	0.27	16.16	0.17	14.87	0.15
FeO <sub>tot</sub>	10.24	0.13	8.18	0.25	2.85	0.18
MnO	nd	nd	0.20	0.09	0.08	0.05
MgO	5.76	0.28	2.77	0.09	0.73	0.05
CaO	10.93	0.37	6.46	0.12	2.34	0.14
Na <sub>2</sub> O	3.45	0.16	4.07	0.15	4.24	0.08
K <sub>2</sub> O	1.99	0.10	1.67	0.06	3.08	0.11
P <sub>2</sub> O <sub>5</sub>	0.51	0.12	0.31	0.06	0.13	0.04
Original sum	99.82		96.66		98.40	

Major element analyses performed by electron microprobe

a: from Iacono-Marziano et al. (2012)

b: from Cadoux et al. (2017), recalculated to 100%

c: from Cadoux et al. (2014, 2017), recalculated to 100%

*n*: number of analyses, and  $\sigma$ : standard deviation of the average of *n* analyses

nd: not determined

These dry glasses were also used to synthesize Br standards characterized in Cadoux et al. (2017)

**Table 2.** Results of the fluid/melt partitioning experiments

	[Br <sup>o</sup> ] <sup>a</sup> (ppm)	fluid/melt mass ratio	[Br] <sub>melt</sub> <sup>b</sup> (ppm)	± 1σ	[H <sub>2</sub> O] <sub>melt</sub> <sup>c</sup> (wt%)	± 1σ	[Br] <sub>fluid</sub> <sup>d</sup> (ppm)	± error (ppm)	D <sub>Br</sub> <sup>f/m</sup>	± error
<b>Experiment #1: Au-Pd capsule, 1200°C, 100 MPa, ~NNO (pH<sub>2</sub> = 2 bars), 24 hours</b>										
Run product # (B for basalt)										
M1-B	72181	0.06	3753	168	n.d.		14298	1595	3.8	4.3
								8		
<b>Experiment #2: Au-Pd capsule, 1200°C, 100 MPa, ~NNO (pH<sub>2</sub> = 2 bars), 24 hours</b>										
M2-B	14251	0.08	9112	464	n.d.		47027	1265	5.2	1.4
								7		
<b>Experiment #3: Au-Pd capsules, 1200°C, 100 MPa, ~NNO (pH<sub>2</sub> = 2 bars), 24 hours</b>										
Run product # (B for basalt, A for andesite, RD for rhyodacite)										
M3-B	24222	0.12	2034	290	3.4	0.0	9370	3845	4.6	2.0
M3-A	24222	0.12	1912	376	4.8	0.1	12298	6227	6.4	3.5
M3-RD	24222	0.12	1426	42	2.9	0.0	16065	1073	11.3	0.9
<b>Experiment #4: Au-Pd capsules, 1060°C, 200 MPa, ~NNO (pH<sub>2</sub> = 2 bars), 48 hours</b>										
M4-A1	999	0.11	69.5	0.1	7.2	0.1	948	138	13.7	2.0
M4-A2	4968	0.11	359	48	7.3	0.1	4439	1498	12.3	4.5
M4-A3	9874	0.11	733	79	7.3	0.2	8396	2462	11.5	3.6
M4-A4	24222	0.12	1960	34	7.2	0.1	16908	2499	8.6	1.3
M4-RD1	999	0.11	69	10	5.2	0.1	662	204	9.3	3.3
M4-RD2	4968	0.11	240	82	4.9	0.2	4968	1437	20.6	9.3
M4-RD3	9874	0.11	591	24	5.4	0.3	8626	966	14.6	1.8
M4-RD4	24222	0.12	1483	242	5.1	0.1	20314	4418	13.7	3.8
<b>Experiment #5: Au capsules, 900°C, 200 MPa, ~NNO (pH<sub>2</sub> = 2 bars), 92 hours</b>										
M5-RD1	999	0.12	79	6	6.8	0.4	701	162	8.6	2.2
M5-RD2	4968	0.11	226	31	6.0	0.3	6307	981	27.9	5.9
M5-RD3	9874	0.11	608	97	6.5	0.5	10113	2704	16.6	5.2
M5-RD4	24222	0.11	1251	214	5.6	0.1	26037	4452	20.8	5.1

Uncertainties on T and P are ± 10°C and ± 2 MPa, respectively.

a: calculated Br content loaded into capsule in H<sub>2</sub>O+NaBr solution

b: measured by LA-ICP-MS in run-product glasses from experiments #1 and 2 (average of 3 to 10 analyses per charge), by SIMS in glasses from experiments #3 to 5 (3-6 analyses per charge)

c: H<sub>2</sub>O content determined by SIMS (5-7 analyses per charge) in run-product glasses from exp. #3 to 5. H<sub>2</sub>O<sub>melt</sub> was not measured in run products from exp. #1 and 2.

d: calculated by mass balance (see supplementary material for details)

1275

1276

**Table 3.** Major element composition (wt%) of the partitioning experiment glassy products

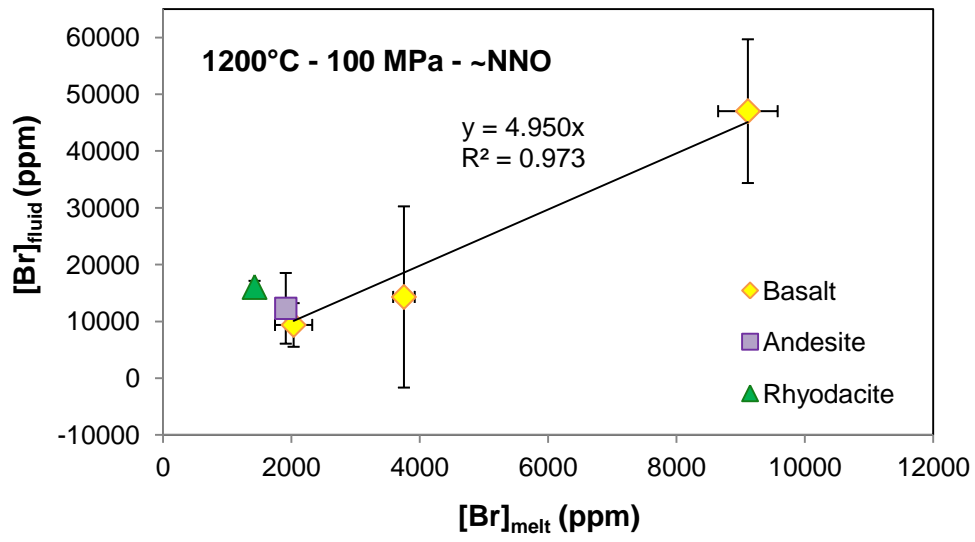
Experiment #	Run product ID	<i>n</i>	SiO <sub>2</sub>	TiO <sub>2</sub>	Al <sub>2</sub> O <sub>3</sub>	FeO <sub>tot</sub>	MnO	MgO	CaO	Na <sub>2</sub> O	K <sub>2</sub> O	P <sub>2</sub> O <sub>5</sub>	Original Sum
1	M1-B	1	48.47 (37)	1.77 (9)	16.79 (18)	10.07 (32)	0.17 (10)	5.83 (20)	10.83 (25)	3.51 (16)	1.98 (14)	0.59 (8)	94.11
		0											
2	M2-B	1	48.36 (29)	1.75 (9)	16.84 (15)	9.89 (30)	0.17 (9)	5.85 (17)	11.01 (31)	3.61 (12)	1.92 (21)	0.60 (9)	94.37
		0											
3	M3-B	7	48.96 (59)	1.65 (16)	17.05 (19)	9.12 (38)	0.17 (12)	6.15 (5)	10.82 (26)	3.60 (10)	2.07 (20)	0.40 (12)	95.01
"	M3-A	7	59.54 (30)	1.27 (14)	16.32 (20)	7.36 (29)	0.10 (8)	2.74 (6)	6.33 (14)	4.46 (8)	1.66 (7)	0.21 (15)	95.14
"	M3-RD	6	71.31 (30)	0.40 (6)	14.77 (18)	2.15 (15)	0.10 (12)	0.72 (3)	2.40 (8)	4.90 (9)	3.20 (10)	0.07 (6)	95.56
4	M4-A1	6	59.50 (33)	1.28 (14)	16.37 (13)	7.66 (41)	0.19 (8)	2.73 (9)	6.35 (6)	4.11 (9)	1.59 (6)	0.22 (12)	93.51
"	M4-A2	6	59.52 (38)	1.36 (17)	16.45 (28)	7.50 (39)	0.18 (9)	2.68 (8)	6.35 (9)	4.14 (11)	1.56 (7)	0.27 (15)	92.77
"	M4-A3	6	59.70 (43)	1.33 (18)	16.55 (10)	7.19 (22)	0.20 (14)	2.66 (5)	6.31 (11)	4.12 (5)	1.61 (10)	0.31 (18)	93.18
"	M4-A4	6	59.44 (54)	1.38 (11)	16.27 (18)	7.73 (19)	0.28 (9)	2.71 (5)	6.34 (14)	4.17 (9)	1.51 (5)	0.16 (20)	92.81
"	M4-RD1	6	71.77 (26)	0.51 (4)	14.85 (20)	2.18 (28)	0.14 (5)	0.69 (4)	2.47 (7)	4.41 (34)	2.88 (19)	0.10 (6)	92.93
"	M4-RD2	5	71.48 (73)	0.48 (9)	14.92 (5)	2.35 (12)	0.05 (5)	0.69 (4)	2.46 (7)	4.51 (7)	2.86 (13)	0.19 (10)	92.35
"	M4-RD3	6	71.49 (61)	0.46 (7)	15.05 (19)	2.28 (25)	0.08 (11)	0.66 (2)	2.45 (11)	4.64 (9)	2.83 (11)	0.05 (8)	92.40
"	M4-RD4	7	71.68 (37)	0.45 (8)	14.63 (22)	2.40 (21)	0.09 (7)	0.71 (4)	2.37 (6)	4.58 (10)	2.90 (10)	0.18 (9)	92.10
5	M5-RD1	8	71.56 (31)	0.49 (8)	14.49 (29)	2.88 (21)	0.06 (8)	0.71 (3)	2.34 (8)	4.35 (8)	3.01 (19)	0.11 (6)	91.79
"	M5-RD2	8	71.47 (39)	0.42 (10)	14.40 (21)	3.01 (30)	0.08 (8)	0.70 (5)	2.41 (11)	4.41 (8)	2.97 (12)	0.11 (10)	92.69
"	M5-RD3	9	71.50 (31)	0.46 (10)	14.39 (13)	2.96 (19)	0.07 (7)	0.72 (4)	2.37 (6)	4.45 (14)	3.00 (19)	0.09 (10)	92.37
"	M5-RD4	7	71.31 (52)	0.41 (11)	14.44 (22)	2.89 (20)	0.05 (6)	0.71 (4)	2.38 (9)	4.58 (9)	3.07 (17)	0.16 (5)	93.19

Major element analyses recalculated to 100%

*n* is the number of analyses per product

Numbers in parentheses indicate one standard deviation of *n* analyses in terms of smallest units cited

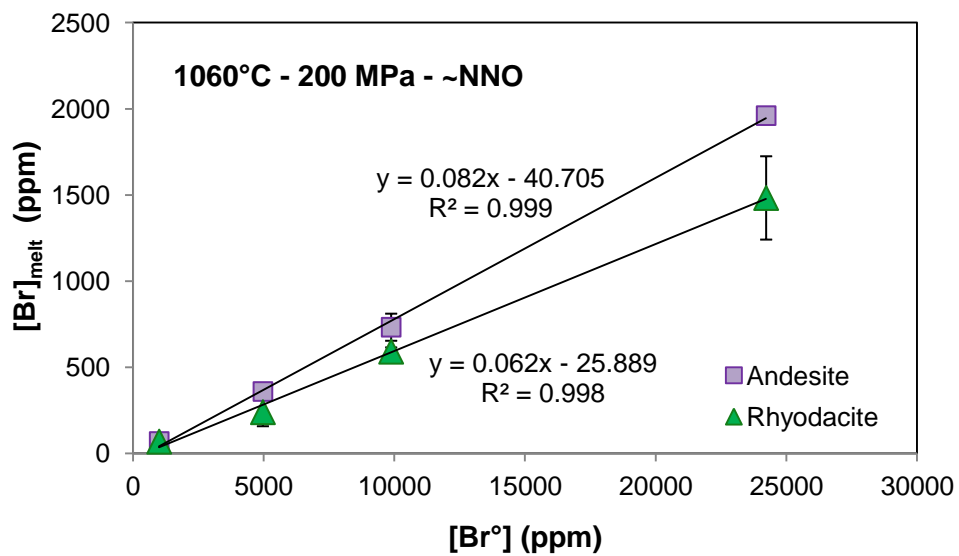
1277 **Figure 1**



1278

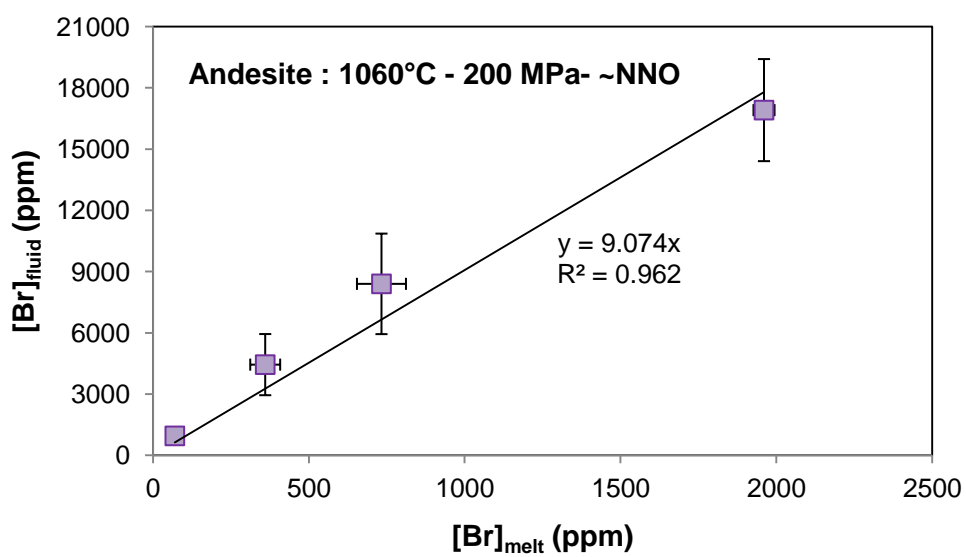
1279

1280 **Figure 2 (a)**



1281

1282 **(b)**



1283

1284

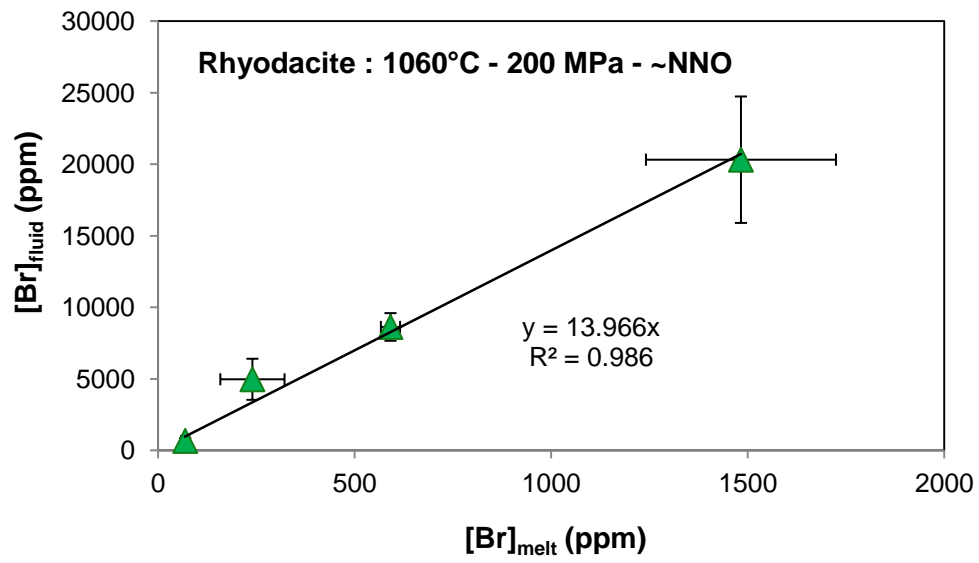
1285

1286

1287

1288

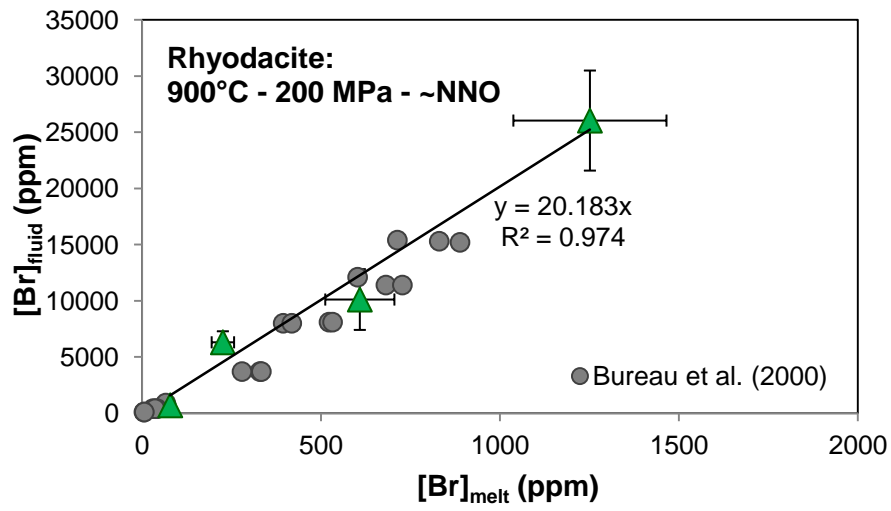
1289 (c)



1290

1291

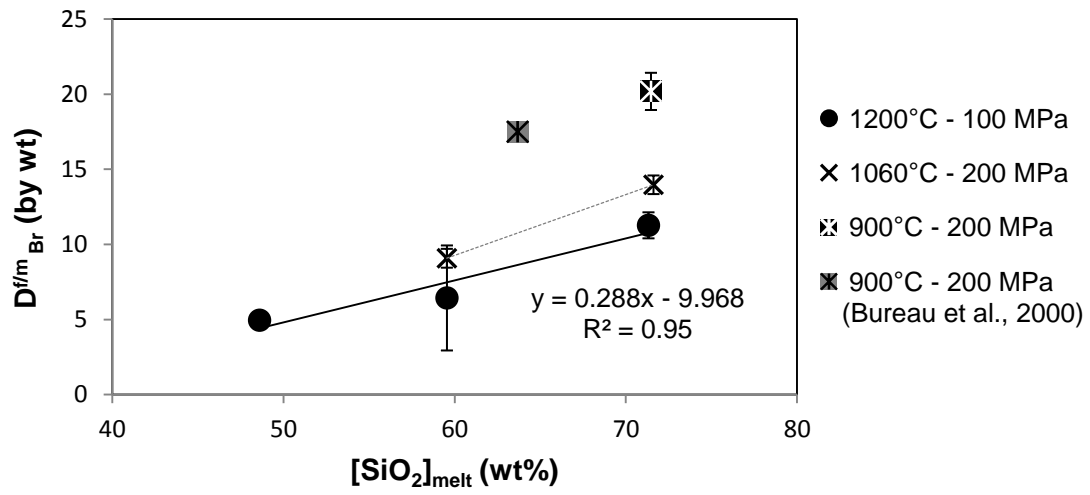
1292 **Figure 3**



1293

1294

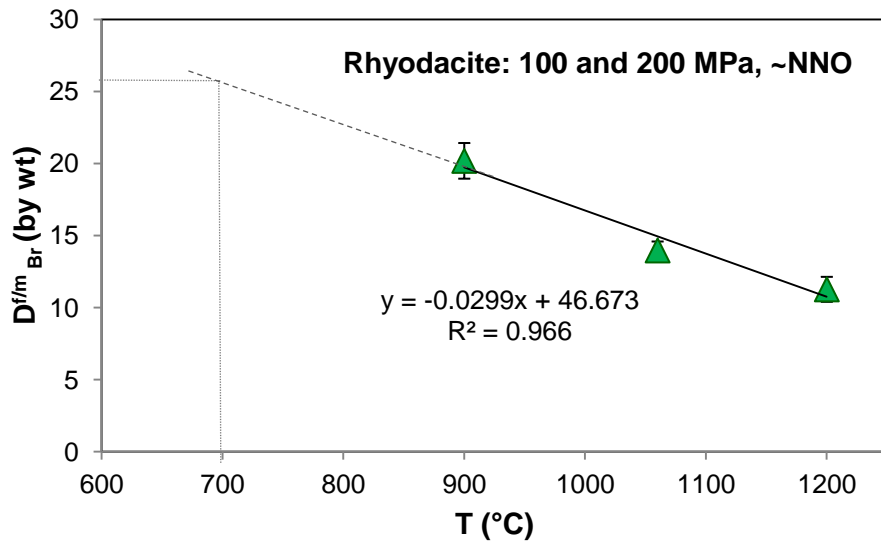
1295 **Figure 4**



1296

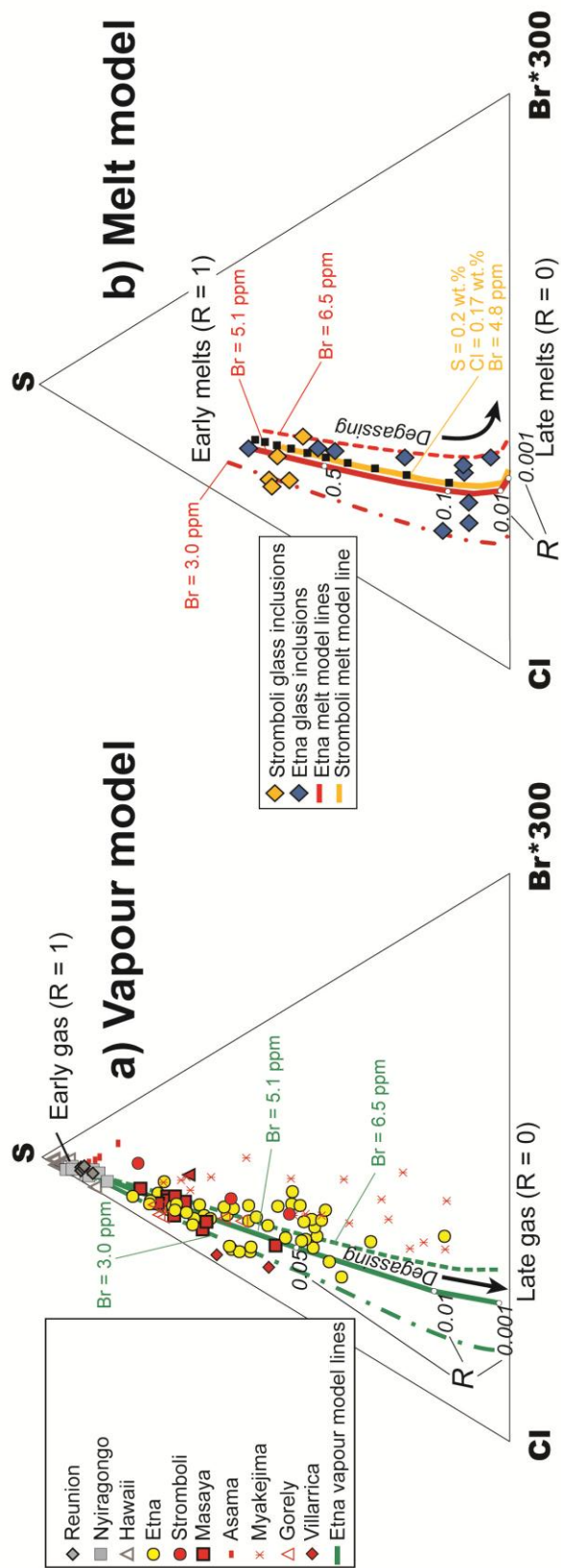
1297

1298 **Figure 5**



1299

1300



**Supplementary material for online publication only**

[Click here to download Supplementary material for online publication only: Figure A.1.pdf](#)

**Supplementary material for online publication only**

**[Click here to download Supplementary material for online publication only: Supplementary Tables\\_rev.xlsx](#)**

**Supplementary material for online publication only**

[Click here to download Supplementary material for online publication only: Supplementary Info\\_final.docx](#)